M 2025

U.PORTO
FEUP FACULDADE DE ENGENHARIA
UNIVERSIDADE DO PORTO

MARKET-AWARE OPTIMAL CONTROL OF ELECTROLYZER SYSTEMS

BRUNO MIGUEL FREITAS DA SILVA
MASTER THESIS IN CHEMICAL ENGINEERING
PRESENTED TO THE FACULTY OF ENGINEERING
OF THE UNIVERSITY OF PORTO

Master in Chemical Engineering

Market-aware optimal control of electrolyzer systems

Master Thesis

of

Bruno Miguel Freitas da Silva

Developed within the course of dissertation

held in

LSRE-LCM – Laboratory of Separation and Reaction Engineering - Laboratory of Catalysis and Materials, ALiCE - Associate Laboratory in Chemical Engineering

Supervisor at FEUP: **Prof.** Diogo Filipe Mateus Rodrigues

Joint supervisor at FEUP: **Prof.** Alexandre Filipe Porfírio Ferreira

FACULTY OF ENGINEERING OF THE UNIVERSITY OF PORTO

DEPARTMENT OF CHEMICAL AND BIOLOGICAL ENGINEERING

July 2025

Acknowledgment

My deepest thanks go to Professor Alexandre Ferreira and Professor Diogo Rodrigues. They recognized my foundational background and potential, and it was their decisive challenge that set me on the path to undertaking this thesis, even when faced with areas like programming that were initially outside my comfort zone. Their belief in my capacity truly inspired me.

Beyond this challenging yet crucial initiation, I owe immense gratitude to Professor Diogo Rodrigues for his continuous, dedicated support. His tireless assistance, insightful feedback, and patient mentorship were foundational to the successful execution and completion of this research.

My deepest gratitude goes to my beloved family. Their unconditional love, unwavering patience, and constant encouragement provided the essential foundation and emotional strength throughout this demanding journey. Knowing I had their steadfast support, whether near or far, was a constant source of motivation and comfort.

Finally, to my incredible friends, thank you for the invaluable balance you brought to my life. Your understanding, laughter, and timely distractions were essential for maintaining perspective and well-being during the intense periods of this work. Your belief in me, coupled with your unwavering friendship, made this achievement more meaningful.

This work was financially supported by Fundação para a Ciência e a Tecnologia, I.P. /MCTES through national funds: LSRE-LCM, UID/50020; and ALiCE, LA/P/0045/2020 (DOI: 10.54499/LA/P/0045/2020).

fct Fundação para a Ciência e a Tecnologia

REPÚBLICA PORTUGUESA

Abstract

As the global energy system transitions toward decarbonization, green hydrogen is emerging as a key vector for storage and sectoral integration. Electrolysis, powered by renewable energy sources, enables sustainable hydrogen production, but economic feasibility depends on operational flexibility in response to electricity market dynamics. This study analyzes two major electrolyzer technologies, Alkaline Water Electrolyzer (AWE) and Proton Exchange Membrane (PEM), using real-world data from REN DataHub on renewable generation and grid electricity prices.

A simulation framework was developed to optimize hydrogen production by adjusting input variables, namely current and cooling water flow, while allowing for dynamic grid power usage. The objective was to maximize hydrogen output and economic return by deciding when to operate, reduce, or halt production based on fluctuating power prices and renewable energy availability. A rolling optimization strategy was employed to account for uncertainty in short-term electricity price forecasts.

The results reveal that both AWE and PEM electrolyzers adapt their operation to electricity price fluctuations. At low prices, they increase production, often using grid electricity; at high prices, they reduce hydrogen output or sell renewable energy to the grid. PEM systems demonstrated greater responsiveness to short-term price variations, maintaining partial operation even during peak pricing due to higher efficiency. AWE systems were more prone to complete shutdowns but were also more stable under constrained output conditions. In scenarios with lower hydrogen prices, both systems significantly reduced operation, prioritizing electricity sales when hydrogen production was no longer economically favourable. These patterns illustrate each system's strategic behaviour in optimizing for profitability under dynamic conditions.

This work highlights the importance of integrating real-time market signals into electrolyzer operation, providing insights for the deployment of hydrogen technologies in flexible, renewable-driven energy systems.

Keywords (theme): Hydrogen production, Electrolyzer optimization, Energy markets, Dynamic optimization, Renewable integration

Resumo

Com a transição global para a descarbonização do sistema energético, o hidrogénio verde surge como um vetor essencial para o armazenamento e integração setorial. A eletrólise, alimentada por fontes de energia renovável, permite uma produção sustentável de hidrogénio, embora a viabilidade económica dependa da flexibilidade operacional face à dinâmica do mercado elétrico. Este estudo analisa duas tecnologias principais de eletrólise, Eletrólise Alcalina (AWE) e Membrana de Troca de Protões (PEM), utilizando dados reais do REN DataHub sobre produção renovável e preços da eletricidade na rede.

Foi desenvolvido um modelo de simulação para otimizar a produção de hidrogénio através do ajuste de variáveis de entrada, nomeadamente a corrente elétrica e o caudal de água de refrigeração, permitindo o uso dinâmico da eletricidade da rede. O objetivo consistiu em maximizar a produção e o retorno económico do hidrogénio, decidindo quando operar, reduzir ou parar a produção com base nas flutuações dos preços da eletricidade e na disponibilidade de energia renovável. Foi adotada uma estratégia de otimização recorrente para integrar a incerteza na previsão dos preços de curto prazo.

Os resultados mostram que ambos os eletrolisadores ajustam o seu funcionamento consoante as variações dos preços da eletricidade. Quando os preços estão baixos, aumentam a produção, muitas vezes recorrendo à eletricidade da rede; quando os preços estão altos, reduzem a produção de hidrogénio, vendendo a energia renovável à rede pública. O sistema PEM revelou maior sensibilidade às variações de preços, mantendo produção parcial durante picos de preços devido à sua maior eficiência. O sistema AWE demonstrou maior tendência para desligamentos completos, mas com comportamento mais estável sob restrições de produção. Em cenários com preço reduzido do hidrogénio, ambos os sistemas reduziram significativamente a operação, favorecendo a venda de eletricidade. Estes padrões ilustram o comportamento estratégico de cada sistema na otimização da rentabilidade em condições dinâmicas.

Este estudo reforça a importância de integrar sinais de mercado em tempo real na operação de eletrolisadores, contribuindo para estratégias mais eficazes de produção de hidrogénio num sistema energético flexível e renovável.

Palavras-chave (tema): Produção de hidrogénio, Otimização de eletrolisadores, Mercados de energia, Otimização dinâmica, Integração de energias renováveis

Declaration

I hereby declare, under word of honour, that this work is original and that all non-original contributions is indicated and due reference is given to the author and source

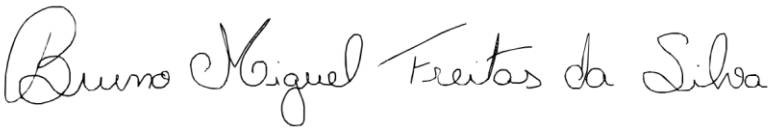

27/06/2025

Index

List of Figures

List of Tables

Notation and Glossary

A_{stack}	Superficial electrolyzer stack area	m^2
C	Thermal capacity	$MJ \cdot K^{-1}$
d_k	Distance between the electrode k and the membrane	mm
$DailyMax_{H_2}$	Maximum daily production possible for the electrolyzer	kg
$E_{act,k}$	Activation energy for the water electrolysis reaction at electrode k	$J \cdot mol^{-1}$
F	Faraday's constant	$C \cdot mol^{-1}$
h	Convective heat transfer coefficient	$W \cdot m^{-2} \cdot K^{-1}$
ΔH	Enthalpy change	$J \cdot mol^{-1}$
ΔH_i	Enthalpy change of component i	$J \cdot mol^{-1}$
$\Delta H_{H_2O}^{in}$	Enthalpy change of water entering the electrolyzer cell	$J \cdot mol^{-1}$
$\Delta H_{H_2O}^{cell}$	Enthalpy change of water in the electrolyzer cell	$J \cdot mol^{-1}$
$\Delta H_{H_2O}^{0}$	Reference enthalpy change of water	$J \cdot mol^{-1}$
I	Current	A
J	Accumulated profit	€
j	Current density	$A \cdot m^{-2}$
j_d	Maximum current density	$A \cdot m^{-2}$
j_{lim}	Limiting current density	$kA \cdot m^{-2}$
$j_{0,k}$	Exchange current density of electrode k	$A \cdot m^{-2}$
$j_{0,k-ref}$	Reference current density of electrode k	$A \cdot m^{-2}$
m	Alkali molar concentration	-
$\dot{m}_{H_2}$	Hydrogen mass flow rate	$kg \cdot s^{-1}$
M_i	Molar mass of component i	$g \cdot mol^{-1}$
N_{cell}	Number of electrolyzer cells	-
$\dot{n}_{H_2}$	Hydrogen molar flow rate	$mol \cdot s^{-1}$
p	Pressure	Pa
p_0	Reference pressure	Pa
p_i	Partial pressure of component i	Pa
P_{ele}	Electrolyzer power	MW
P_{grid}	Grid power	MW
P_{solar}	Solar power	MW
P_{wind}	Wind power	MW
$Price_{H_2}$	Hydrogen sell price	$€ \cdot kg^{-1}$
$Price_{grid}$	Grid electricity price	$€ \cdot MWh^{-1}$
q	Volumetric water flow rate	$cm^3 \cdot s^{-1}$
Q_{conv}	Convection heat loss rate	W
Q_{ele}	Electric heat loss rate	W
Q_{loss}	Total heat loss through convection and radiation rate	W
q_{max}	Maximum volumetric water flow rate	$cm^3 \cdot s^{-1}$
Q_{rad}	Convection heat loss rate	W
ΔQ_{H_2O}	Water heat absorbed rate	W
$\mathcal{R}$	Gas constant	$J \cdot mol^{-1} \cdot K^{-1}$
R_k	Electrode k resistance	Ω
$R_{\text{KOH-bubble}}$	Electrolyte resistance	Ω
R_{mem}	Membrane resistance	Ω
R_{ohm}	Ohmic resistance	Ω

R_{ion}	Ionic resistance	Ω·m^2
S_k	Electrode k area	m^2
S_m	Membrane area	m^2
T	Electrolyzer temperature	K
T_0	Reference temperature	K
T_{amb}	Ambient temperature	K
T_{nom}	Nominal temperature	K
t_f	Final operation time	s
t_{day}	Time within a day	s
$U_{act,k}$	Activation overpotential of electrode k	V
U_{cell}	Cell voltage	V
U_{ohm}	Ohmic overpotential	V
U_{rev}	Reversible voltage	V
U_{rev}^0	Standard conditions reversible voltage	V
U_{stack}	Stack voltage	V
U_{th}	Thermoneutral voltage	V
z	Number of electrons transferred per mole of hydrogen	-

Greek Letters

α_k	Transfer coefficient for electrode k	-
$\alpha_{\mathrm{H_2O}}$	Water activity	-
β	Minimum daily hydrogen production ratio	-
δ_k	Electrode k thickness	m
δ_m	Membrane thickness	m
ε_{stack}	Surface emissivity of the stack	-
η	Overpotential	V
η_F	Faraday efficiency	-
θ	Ratio of electrode surface covered by generated bubbles	-
λ_m	Membrane water content	-
φ	Membrane porosity	-
ω	Alkali mass fraction concentration	-
ρ_{H_2O}	Water density	g·cm^{-3}
σ	Stefan–Boltzmann constant	J·K^{-1}
σ_k	Electrode k conductivity	S·m^{-1}
σ_{KOH}	Electrolyte conductivity	S·m^{-1}
$\sigma_{KOH-bubble}$	Electrolyte conductivity with generated bubbles effect	S·m^{-1}
τ_m	Membrane tortuosity	-

Indexes

i	Reaction component
k	Type of electrode

List of Acronyms

AEM	Anion Exchange Membrane
AWE	Alkaline Water Electrolyzer
CAPEX	Capital Expenditure
MPC	Model Predictive Control

PEM	Proton Exchange Membrane
SOE	Solid Oxid Electrolyzer

1. Introduction

1.1. Framing and presentation of the work

The global push for decarbonization, emphasized by the United Nations, has accelerated hydrogen technology development, valued both as an industrial raw material and a clean energy carrier. Green hydrogen, produced via water electrolysis driven by renewable power, is a key enabler of the energy transition. As electricity grids integrate more variable renewable energy sources, hydrogen production helps absorb surplus electricity and supports grid stability.

Electrolyzers, which split water into hydrogen and oxygen using electricity, are central to this shift. Alkaline Water Electrolyzers (AWE) and Proton Exchange Membrane (PEM) electrolyzers are the most widely used, each with distinct operational characteristics suited to different energy and market contexts.

Despite growing interest and increasing deployment, challenges remain in the economic and technical viability of electrolyzers, especially in real-time electricity markets. High manufacturing costs and sensitivity to fluctuating electricity prices, due to renewable intermittency, grid congestion, and demand changes, limit integration and scalability. Fixed control strategies often fail to capture market dynamics, leading to unrealistic assumptions.

Dynamic optimization offers a powerful way to improve electrolyzer operation under variable conditions by balancing profitability and operational constraints. Techniques like Model Predictive Control, nonlinear programming, and stochastic optimization enable continuous adjustments based on electricity price forecasts and renewable power availability, enhancing hydrogen yield, reducing costs, and increasing flexibility.

This dissertation investigates market-aware optimal control for AWE and PEM electrolyzers under identical conditions. Rather than focusing on design or hardware differences, the study emphasizes operational behaviour in response to real-time market signals, such as electricity prices and renewable power availability. Using model-based simulation and dynamic optimization, it evaluates their responsiveness and suitability under fluctuating market signals. The results provide insights into practical integration strategies for renewable-rich grids and support cost-effective hydrogen production.

Using real-time simulation data, this study assesses the flexibility and integration potential of AWE and PEM electrolyzers to meet evolving energy demands. Three case studies simulate real-world market conditions, examining system responses to fluctuating electricity and hydrogen prices and intermittent renewable energy generation, providing a qualitative assessment of each technology’s adaptability.

1.2. Contribution of the author to the work

The author contributed to this work through the development of dynamic optimization codes in Python using the CasADi package, as well as the modelling and parameterization of the electrolyzer systems using Python and Excel to define and test their performance models. Additionally, the author was responsible for acquiring and processing up-to-date real-time data, which was integrated into the simulation framework to reflect realistic operating conditions and market dynamics.

1.3. Organization of the dissertation

This dissertation is subdivided in seven chapters.

The first chapter, Introduction, presents the context and motivation for the research, highlighting the role of electrolyzer systems in the energy transition and the importance of optimizing their operation under dynamic market conditions. It also introduces the main objectives and scope of the work.

The second chapter, Context and State of the Art, provides a detailed description of AWE and PEM electrolyzer systems, alongside an overview of other relevant technologies. Key limitations and assumptions are identified and applied to simplify the modelling process. The chapter also discusses the principles of dynamic optimization and introduces CasADi as a computational tool for implementing optimal control strategies in electrolyzer operation.

The third chapter, Modelling and Simulation Framework, presents the model equations, optimization constraints, and objective functions applied to both electrolyzer systems. It outlines the specific goals of the optimization problem and details the simplifications and assumptions incorporated into the models. Additionally, relevant data used in the design and parameterization of each system are discussed.

The fourth chapter, Results and Discussion, presents the simulation results and provides a comprehensive analysis of the operational performance of both electrolyzer systems under different market scenarios. It examines their dynamic behaviour, responsiveness to fluctuating electricity prices, and overall flexibility.

The fifth chapter, Conclusion, summarizes the main findings, outlines the study's contributions, and suggests directions for future research in electrolyzer operation and optimization.

The sixth chapter, Assessment of the Work Done, provides a concise overview of the completed objectives and evaluates their relevance to sustainable development goals.

2. Context and State of the art

2.1. Electrolyzer technology overview

Electrolyzers represent the most established and widely recognized renewable energy technology for producing green hydrogen, which has an important role in the sustainability of future energy transition. Water electrolysis technologies for hydrogen production can generate it with high purity to be able to meet its growing demand for circular economy and future sustainable solutions on clean energy systems [1]. While their development is deeply rooted in scientific and engineering advancements, an increasing technology maturing is evident over the years, with the development of different types of electrolyzers for the current market targets and needs. AWE, PEM, anion exchange membrane (AEM) and solid oxide electrolyzers (SOE) are being highlighted with their market readiness and viability for their energy applications in the era of renewable energy market. PEM and AWE are relatively mature, with predictable behaviour and environmental performance and a well-established manufacturing process regarding its system components and material usage. On the other hand, SOE and AEM still present some technical and functional challenges, namely degradation issues and manufacturing process which have an important role for the overall stack performance and stability, durability, and its limitations to different scenarios [2]. Nevertheless, the emergence of these different kinds of hydrogen production technologies also contributes to their integration and engagement in the current market. This increasing adoption of electrolyzers in industry, not only as a final product but also as a potential sub-application, is the fuel for this maturing run. SOE is recognized as a future ally for industries with high heat workloads since this technology operates usually in the range of 600 °C up to 1000 °C, coupled with its easy scalability for different demands. SOE are also recognized for their syngas generation potential, due to their capability to perform co-electrolysis of CO_2 and water, resulting in syngas production, which reinforces market opportunity for fuel power plants to contribute to the industrial decarbonization goals [3]. These capabilities of SOE could encourage these target industries to invest in the maturing and advancement of this technology, as they still face major issues such as long-term durability, reliability, and material degradation due to high temperature exposure, which limits their efficiency and lifespan.

2.2. AWE and PEM

The focus on this work will be on optimization of the two widely recognized, most mature and commercially available technologies for hydrogen production, AWE and PEM. AWE is the most established technology, with a long history of industrial use, being recognized by its maturity in electrolysis processes. Its module is composed by two

electrodes immersed in an alkaline solution of potassium or sodium hydroxide. These electrolytes operate with a typical concentration of hydroxide ions around 25-40% [4]. There is a physical division between both electrodes by a porous membrane and the separator is crucial for allowing a restrictive flow of OH^- ions and for imposing the flux of electrons by the external circuit. At the cathode, water undergoes reduction, producing hydroxide ions and hydrogen gas. Subjected to an externally induced electric field, the ion conduction occurs within the electrolyte, passing across the diaphragm to the anode. Upon arrival at the anode, hydroxide ions undergo oxidation to form oxygen gas [5]. In Table 2.1 and Figure 2.1, the reactions which occur in each electrode previously described are represented:

Table 2.1 - Half-reactions in cathode and anode side for AWE

Cathode:	$4H_2O(l) + 4e^- \rightarrow 2H_2(g) + 4OH^-(aq)$
Anode:	$4OH^-(aq) \rightarrow O_2(g) + 2H_2O(l) + 4e^-$

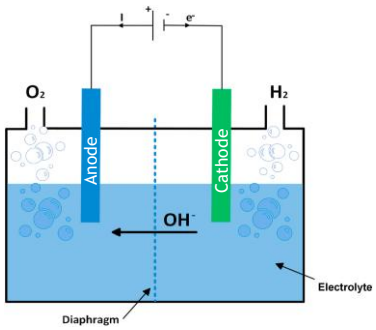

Figure 2.1 - Cell operation diagram of an AWE [4]

The electrodes surface is designed to facilitate the bubbles formed during the water electrolysis. These gas bubbles will continue to grow coalescing with surrounding ones or by diffusion of the gases produced, blocking active sites, creating electron resistance, and impacting the overall electrolyzer efficiency and compromising hydrogen purity [6]. AWE can produce hydrogen with over 99.999% purity at ambient temperature. The electrodes are built with non-noble metals, typically nickel or iron, which lower their CAPEX. However, this technology is very restricted with limited current density, lower efficiency compared with other technologies, and corrosion associated with the alkaline electrolyte. Additionally, the lengthy start-up time and slow load response makes it challenging for AWE to adjust to intermittent renewable energy sources.

To address the limitations of AWE, PEM electrolysis technology emerged, revolutionizing the hydrogen production industry. In this technology configuration, it is mandatory to feed only deionized water to the cell. The electrolyte is a polymer membrane, known for its high proton conductivity, low gas crossover, small thickness, and high-pressure operation, which contrasts with the restrictive nature of the AWE. Deionized water is

supplied to the anode to be oxidized. The hydrogen ions cross over the membrane to be collected in the cathode and to be released in its gas form after reacting with the electrons transported via the external circuit [4]. In Table 2.2 and Figure 2.2, the reactions in each electrode, cathode and anode, respectively, are represented.

Table 2.2 - Half-reactions in cathode and anode side for PEM

Cathode:	$4H^+(aq) + 4e^- \rightarrow 2H_2(g)$
Anode:	$2H_2O(l) \rightarrow O_2(g) + 4H^+(aq) + 4e^-$

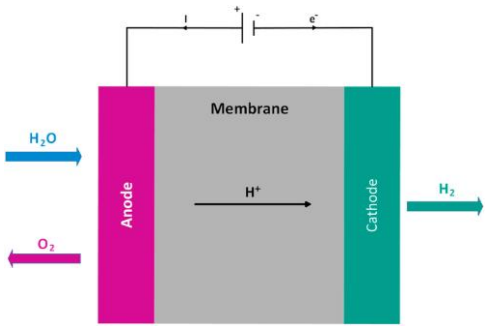

Figure 2.2 – Cell operation diagram of a PEM [4]

The low gas crossover allows a wide range of power inputs and fluctuations with fast response from the cell. Because the electrolyte in PEM electrolyzers is a solid polymer rather than a liquid as in alkaline water electrolyzers (AWE), proton crossover closely follows changes in the supplied power without the lag caused by inertia seen in AWE systems. In alkaline electrolyzers running at low power levels, production rates of hydrogen and oxygen decline, yet hydrogen permeability through the diaphragm remains steady. This leads to an increased concentration of hydrogen on the anode (oxygen) side, which poses safety risks and reduces efficiency. Conversely, PEM electrolysis maintains efficient operation over a broad range of power densities and can even operate above its nominal power (by 10–100%) thanks to the Nafion® membrane's low hydrogen permeability, thereby improving overall performance and efficiency. However, this configuration suffers from high capital costs, since PEM relies on precious metal catalysts (platinum and iridium) to achieve efficient reactions and to handle the acidic regime provided by the membrane, leading to the corrosion of the catalysts, current collector, and separator plates, reducing its lifespan [7].

Both technologies face their drawbacks, but each one offers distinct advantages that make them suitable for different applications. AWE remains a cost-effective and well-established choice for hydrogen production, particularly in industries where high purity and long-term stability are required. However, its limitations in efficiency, slow dynamic response, and sensitivity to corrosion restrict its adaptability to modern energy demands. On the other hand, PEM electrolysis presents a highly responsive and efficient alternative,

capable of handling variable renewable energy inputs with ease. Despite its higher capital costs and reliance on noble metals, ongoing research and technological advancements aim to reduce these constraints, making PEM a strong candidate for the future of sustainable hydrogen production. Ultimately, selecting between AWE and PEM is determined by the specific operational and financial constraints of the application, as both technologies continue to evolve in the pursuit of cleaner and more efficient energy solutions.

2.3. Limitations and Assumptions

To enable tractable implementation of the simulation framework, several assumptions and simplifications were made regarding the physical and operational characteristics of the electrolyzer systems. For the electrochemical water splitting process to work efficiently, several obstacles must be overcome, all of which require a steady supply of electrical energy. These obstacles include electrical resistance in the circuit, which slows down the current flow and reduces the overall efficiency of the system, while also leading to waste of energy generating heat according to the Ohms law. These resistances derive from the electrodes to the connection circuits, being determined by the dimensions and specifications of the materials [8].

Another major challenge is presented by the activation energy of the electrode reactions. These energies act as kinetic barriers that must be overcome for the reaction to proceed, contributing to what is often termed reaction resistance or overpotential. In both AWE, focusing on the oxygen evolution reaction, and PEM electrolyzers, concerning the hydrogen evolution reaction, a significant amount of energy is required to initiate these processes. Should these activation energies be too high, a larger applied voltage will be necessary, directly resulting in lower operational efficiency.

In addition, ionic transfer resistance within the electrolyte also limits performance. The ions (like OH^- in alkaline systems or H^+ in PEM systems) need to move through the electrolyte to reach the electrodes. If the electrolyte is too resistant to ion movement, this slows down the reaction and raises the energy required to drive the process. Factors like electrolyte type, concentration, and distance between electrodes impact in the ionic flow [8].

Mass transfer plays a key role in water electrolysis systems, affecting gas bubble behaviour, dissolved gas diffusion and overall efficiency. Gas contamination, a key safety and performance factor, is affected by the movement of hydrogen and oxygen through the electrolyte and separator. The Sherwood and Nusselt numbers help describe convective mass and heat transfer, which impact bubble detachment, electrolyte circulation, and reactant distribution. These effects shape the electrolysis process by determining how efficiently

reactants reach the electrodes and how quickly products are removed, ultimately influencing cell voltage, energy consumption, and gas purity [9].

To improve efficiency, it is important to consider all these barriers. From a thermodynamic standpoint, it is essential to determine the minimum energy needed to drive the water splitting reaction. But in practice, kinetic factors, like the overpotentials at the electrodes and how effective the catalysts are, influence the actual energy needed. Moreover, transport phenomena, including ion migration and current distribution, significantly influence the process efficiency. By simultaneously optimizing these elements, energy losses can be minimized, leading to enhanced electrolyzer performance. [8].

To simplify the model to compute, some considerations were made, and limitations were included. Electrical resistances, diffusion, bubble detachment, and ion transfer resistance were not considered. Gases were considered as ideal, since at lower pressures, below 30 bar, the ideal gas assumption is reasonably accurate, with deviations typically under 10 mV [10]. The water feed is considered as pure water, deionized for the PEM. The operational pressure was considered atmospheric (1 atm) since the efficiency of electrolyzer cells operating under pressure is not significantly higher compared to those operating at ambient pressure. Operating under pressure increases the amount of gas that dissolves in the electrolyte, and it also demands a more durable diaphragm to handle the added stress [8].

2.4. Dynamic optimization

Dynamic optimization is a key concept in control theory and decision making, particularly on systems that evolve over time. It is a mathematical approach useful in scenarios where decisions made at one point affect the future states, requiring a strategy that accounts for both immediate and long-term objectives. This type of optimization is widely applied in control systems, economics, and engineering where processes are led by dynamic constraints and uncertainties.

The principle in dynamic optimization is breaking down a complex, multi-stage problem into smaller and more manageable subproblems. This is often done using recursive methods, ensuring that optimal decisions at each stage contribute to the overall best results. The approach is specifically relevant for energy systems, such as electrolyzers, where operating conditions change over time. By optimizing variables like power input, temperature, and water intake dynamically, efficiency can be maximized while minimizing energy losses and overall system costs and ensuring its longevity [11].

A system in a transient state, such as a time-dependent one, can be mathematically represented using differential equations that describe how its variables evolve over time.

For instance, if the system's state is given by x and time denoted by t, its behaviour is defined by two main components: a differential equation governing its dynamics, and a boundary condition that sets specification constraints, as illustrated in Equation (2.1).

$$\frac{dx(t)}{dt} = f(x(t)), \qquad x(t_0) = x_0 \tag{2.1}$$

In dynamic optimization, the number of boundary conditions should be equal to the number of dynamic variables within the system. The approach to solving differential equations varies based on the problem's complexity. Simple problems may be tackled with analytical methods such as direct integration or Laplace transforms. For more intricate problems, numerical techniques like Euler's method, Runge-Kutta methods, or discretization strategies are used to find approximate solutions with high precision [11]. During transient periods, the system adapts to changes or disturbances, such as changes in input or non-equilibrium starting conditions. This phase can be analysed by observing how the solution to the differential equations develops over time.

2.5. CasADi

In this work, CasADi was used to formulate and solve the dynamic optimization problem. CasADi is an open-source software tool designed for nonlinear optimization and optimal control. It provides a powerful and flexible framework for solving dynamic optimization problems, including both continuous and discrete systems. CasADi is particularly well-suited for handling complex mathematical models, such as differential equations and dynamic systems, and offers various solvers for large-scale optimization problems. It supports symbolic expressions, making it easier to define optimization problems and to analyse their structure. Through its interface with multiple solvers, such as IPOPT and BlockSQP, CasADi can efficiently solve large and nonlinear optimization problems, which are common in fields like control engineering and applied mathematics [12][13].

In dynamic optimization, CasADi is helpful for setting up and solving optimal control problems, including those involving differential-algebraic equations, by combining symbolic modelling with powerful numerical tools. A key feature that enables this capability is automatic differentiation, which allows for the efficient and accurate computation of derivatives required by gradient-based optimization algorithms. Its symbolic expression framework enables users to define complex dynamic systems efficiently, while its numerical solvers handle the resulting optimization problems effectively. This combination allows for the analysis of both transient and steady-state behaviours in dynamic systems, making CasADi a valuable tool for researchers and practitioners in control engineering and applied mathematics.

3. Modelling and Simulation Framework

As mentioned, this work is focused on the AWE and PEM electrolyzers, and due to their technical and operational differences, two models were created to represent the production of hydrogen and the energy balance for these systems.

This chapter details the mathematical models developed to simulate the operation of AWE and PEM electrolyzers. Each model accounts for the specific physical, electrochemical, and thermodynamic behaviours of the two technologies, as well as the analysis of performance in terms of hydrogen production rate and energy losses. The models were built using Python, and implement thermodynamic equations, overpotential models, and empirical correlations found in recent literature.

3.1. Electrolyzer Design and Sizing

Both models consider the electrolyzer as a stack composed of multiple individual electrolytic cells connected in series. To ensure consistency and enable a fair comparative analysis between the two technologies, the total system power was fixed at 1 MW for both the AWE and PEM systems.

The electrolyzer power can be described as the following Equation (3.1):

$$P_{ele} = U_{stack} I \tag{3.1}$$

where P_{ele} is the target system power (1 MW), U_{stack} is the voltage of the electrolytic stack, and I is the current applied to each cell (identical across the stack since the cells are connected in series). Given that the cells are connected in series, the stack voltage can be modelled as shown in Equation (3.2):

$$U_{stack} = U_{cell} N_{cell} \tag{3.2}$$

where U_{cell} is the voltage of a single electrolytic cell (which will be calculated from the electrochemical model), and N_{cell} is the number of electrolytic cells.

The power equation can be then rearranged to include the number of cells, as expressed by Equation (3.3):

$$P_{ele} = U_{cell}\, N_{cell} I \tag{3.3}$$

The operating current I was selected based on typical values reported in the scientific literature and datasheets from commercial electrolyzer manufacturers. This ensures that the modeled system operates within realistic industrial parameters, allowing for meaningful performance comparisons and scaling estimates. Table 3.1 presents the electrolyzer design parameters.

Table 3.1 – Electrolyzer design parameters

Model	Current (I)	Voltage (V)	Length (m)	Diameter (m)	Volume (m^3)
AWE	2500 [14][15]	400 [14][15]	15 [16]	0.8 [16]	7.5
PEM	4000 [17]	250 [17]	2 [18]	0.71 [18]	0.8

Rearranging Equation (3.2), a new expression for the number of cells is obtained as shown in Equation (3.4):

$$N_{cell} = \frac{P_{ele}}{U_{cell} I} \tag{3.4}$$

Since U_{cell} depends on factors such as temperature, pressure, and current density, the number of cells was calculated based on the optimal operating conditions, specifically at a temperature of 60 °C and at the maximum current defined for each technology. These conditions were chosen as they represent typical optimal performance points for both AWE and PEM electrolyzers, ensuring high efficiency and production. The resulting number of cells ensures the stack configuration delivers a total system power of 1 MW under these reference conditions. The electrolyzer stack configuration parameters are summarized in Table 3.2.

Table 3.2 – Electrolyzer stack configuration parameters

Model	Number of cells	Cell Area (m^2)
AWE	181	0.5
PEM	159	0.4

While the electrolyzer model was designed based on specific nominal current and voltage targets, the physical constraint of having an integer number of cells required rounding the calculated cell count. Consequently, the actual operational current and voltage depicted in the model's output figures reflect these adjusted values, rather than the initial exact targets.

Three sources of electrical power were considered for the electrolyzer systems: solar energy P_{solar}, wind energy P_{wind}, and the electrical grid P_{grid}, as shown in Equation (3.5). The primary objective was to rely on renewable sources, solar and wind, whenever possible. These sources were prioritized based on their availability, with solar and wind contributing to the electrolyzer load if sufficient generation was available. In periods of low renewable output, electricity was supplemented by the grid to ensure continuous operation. This hybrid supply strategy aims to maximize the use of clean energy while maintaining system reliability. When electricity is purchased from the grid, the power drawn P_{grid} is considered

a negative value, reflecting its negative impact on system profitability. Conversely, if there is a surplus of generated renewable energy beyond the electrolyzer's demand, P_{grid} is recorded as positive, representing a potential opportunity for energy export or financial credit.

$$P_{ele} = P_{solar} + P_{wind} - P_{grid} \tag{3.5}$$

The design and sizing of the PEM and AWE electrolyzer stacks, including stack diameter and overall dimensions, were based on data from existing commercial electrolyzers. These parameters were selected to reflect practical, real-world configurations reported in the literature, ensuring that the simulated systems closely represent current industry standards in terms of physical size and design. Accurately defining the stack diameter and overall size was essential for estimating the superficial area of the electrolyzer, which directly impacts the heat exchange characteristics with the environment. Moreover, the cell active area within the stack influences key electrochemical parameters such as current density and cell voltage. Together, these geometric factors are critical for accurately modelling both the thermal behaviour and electrolysis performance of the systems. Table 3.3 presents the electrolyzer dimensions.

Table 3.3 – Electrolyzer dimensions

Model	Superficial Area (m^2)
AWE	37.6
PEM	4.5

To accurately simulate the performance of both AWE and PEM electrolyzers, mathematical models were developed based on electrochemical theory and empirical data. These models aim to represent the voltage behaviour of a single electrolytic cell under various operating conditions, incorporating key loss mechanisms such as activation overpotentials, ohmic resistance, and thermodynamic effects. The following sections present the equations used to describe the cell voltage, energy balance, and hydrogen production rate for each technology, with all parameters selected to reflect realistic operational conditions and supported by data from the literature and industrial sources.

3.2. AWE Model

With the stack configuration defined, the next step involves modelling the electrochemical behaviour of a single alkaline electrolytic cell. The following equations describe the voltage components and system parameters used to calculate the cell voltage and hydrogen production rate. These expressions incorporate thermodynamic, kinetic, and

ohmic losses specific to alkaline electrolysis, and are essential for accurately estimating the overall system performance.

The cell voltage U_{cell} is calculated as the sum of the reversible voltage U_{rev}, the activation overpotentials at the anode $U_{act,a}$ and cathode $U_{act,c}$, and the ohmic losses U_{ohm} within the system [19], as expressed in Equation (3.6). Although other phenomena, such as concentration overpotential, can influence the overall voltage, these effects were neglected in this study to simplify the model and due to the time constraints of the dissertation.

$$U_{cell} = U_{rev} + U_{act,a} + U_{act,c} + U_{ohm} \tag{3.6}$$

3.2.1. Reversible Voltage

The reversible voltage U_{rev} is the minimum theoretical voltage needed to drive a redox reaction to occur and is dependent on temperature, pressure, and water activity. This value is calculated by Nernst equation (3.7), as follows:

$$U_{rev} = U_{rev}^{0} + \frac{\mathcal{R}T}{2F} \ln\left[\frac{\left(p - p_{H_2O}\right)^{1.5}}{\alpha_{H_2O}}\right] \tag{3.7}$$

where U_{rev}^{0} is the standard conditions reversible voltage, which is also influenced by the stack temperature T as shown in the following equation, $\mathcal{R}$ is the gas constant, F is Faraday's constant, p is the operating pressure, $p_{\mathrm{H_2O}}$ is the water vapour partial pressure, and $\alpha_{\mathrm{H_2O}}$ is the water activity in the range 0-150 °C [19]. The expression for U_{rev}^{0} is given by Equation (3.8):

$$U_{rev}^{0} = 1.50342 - 9.956 \times 10^{-4} T + 2.5 \times 10^{-7} T^{2} \tag{3.8}$$

$p_{\mathrm{H_2O}}$ and $\alpha_{\mathrm{H_2O}}$ are expressed by the empirical formulas which are dependent on m, alkali molar concentration, and stack temperature T, as shown in Equations (3.9) and (3.10), respectively [19]:

$$\begin{aligned} \log p_{H_2O} = {} & -0.01508m - 0.0016788m^{2} + 2.25887 \times 10^{-5} m^{3} + \\ & \left(1 - 0.0012062m + 5.6024 \times 10^{-4} m^{2} - 7.8228 \times 10^{-6} m^{3}\right) \times \\ & \left(35.4462 - \frac{3343.93}{T} - 10.9 \log T + 0.004165T\right) \end{aligned} \tag{3.9}$$

$$\log \alpha_{\mathrm{H_2O}}\,(\mathrm{KOH}) = -0.02255m + 0.001434m^{2} + \frac{\left(1.38m - 0.9254m^{2}\right)}{T} \tag{3.10}$$

The alkali molar concentration m is expressed by the following Equation (3.11):

$$m = \frac{\omega}{56.105}\left(183.1221 - 0.56845T + 984.5679 \exp\left(\frac{\omega}{1.1596277}\right)\right) \tag{3.11}$$

where ω is the alkali mass fraction concentration [19].

3.2.2. Activation Overpotential

The activation overpotential is the additional voltage required beyond the equilibrium potential to overcome the activation energy barrier for electron transfer at the electrode surface, enabling the electrochemical reaction to proceed at a practical rate, is calculated separately for each electrode as shown in Equations (3.12) [19]:

$$U_{act,k} = \frac{\mathcal{R}T}{2\alpha_k F} \ln\left[\frac{j}{j_{0,k}(1-\theta)}\right] \tag{3.12}$$

where j is the current density, $j_{0,k}$ is the exchange current density of the electrode, with $k = a$ for the anode and $k = c$ for the cathode, θ is the ratio of electrode surface covered by generated bubbles, and α_k is the transfer coefficient of the electrode. It is important to mention that these parameters are specified for the electrode's material, in this case nickel, and are calculated by Equations (3.13) to (3.17) [19]:

$$\theta = \left[-9725 + 182\frac{T}{T_0} - 84\left(\frac{T}{T_0}\right)^2\right]\left(\frac{j}{j_{lim}}\right)^{0.3} \frac{p}{p - p_{H_2O}} \tag{3.13}$$

$$\alpha_a = 0.07835 + 0.001T \tag{3.14}$$

$$\alpha_c = 0.1175 + 0.00095T \tag{3.15}$$

$$j_{0,a} = 0.9\left(\frac{p}{p_0}\right)^{0.1} \exp\left[-\frac{42000}{\mathcal{R}T}\left(1 - \frac{T}{T_0}\right)\right] \tag{3.16}$$

$$j_{0,c} = 1.5\left(\frac{p}{p_0}\right)^{0.1} \exp\left[-\frac{23000}{\mathcal{R}T}\left(1 - \frac{T}{T_0}\right)\right] \tag{3.17}$$

where p is the operating pressure, p_0 the reference pressure, T_0 the reference temperature, and j_{lim} is the limiting current density under full bubble coverage of the electrode [20].

3.2.3. Ohmic Overpotential

In an electrolyzer, the flow of electric current through various cell components, such as the electrodes, electrolyte, and membrane, encounters inherent electrical resistance. This resistance leads to a voltage drop known as ohmic overpotential. Analogous to an electric circuit, where resistive elements cause energy losses in the form of heat, the electrolyzer exhibits similar behaviour due to ionic and electronic resistances. Ohmic overpotential increases linearly with current as shown in the following Equation (3.18) [19]:

$$U_{ohm} = R_{ohm} I = (R_a + R_c + R_{\text{KOH-bubble}} + R_{mem}) \times I \tag{3.18}$$

where R_{ohm} is the ohmic resistance, I is the current, and R_a, R_c, $R_{\text{KOH-bubble}}$, R_{mem} the anode, cathode, electrolyte and membrane resistances, respectively.

The electrode resistance, R_k with $k = a$ for the anode and $k = c$ for the cathode, is given by the following Equation (3.19) [19]:

$$R_k = \frac{1}{\sigma_k}\left(\frac{\delta_k}{S_k}\right) \tag{3.19}$$

where δ_k and S_k are the thickness and area of the electrode. σ_k represents the electrode conductivities, which are equal due to being made from the same material, nickel, so the electrical conductivity of nickel σ_{Ni} is calculated using the following Equation (3.20) [19]:

$$\sigma_a = \sigma_c = \sigma_{Ni} = 60000000 - 279650T + 532T^2 - 0.38057T^3 \tag{3.20}$$

The electrolyte resistance, accounting for the effect of gas bubbles (denoted as $R_{KOH-bubble}$), is determined by the intrinsic resistance of the electrolyte R_{ele} and a correction term representing the influence of the bubbles. The intrinsic resistance R_{ele} is calculated as shown in Equation (3.21) [19]:

$$R_{ele} = \frac{1}{\sigma_{KOH}}\left(\frac{d_a}{S_a} + \frac{d_c}{S_c}\right) \tag{3.21}$$

where d_a, d_c are the distances between the electrode and the membrane, for anode and cathode respectively, and σ_{KOH} is the electrolyte conductivity, with this parameter being related to the electrolyte concentration and temperature, as shown in Equation (3.22) [19]:

$$\begin{aligned}\sigma_{KOH} = -2.041m + 5.332mT \times 10^{-3} + 2.072 \times 10^{2} mT^{-1} - \\ 2.8m^2 \times 10^{-3} + 1.043m^3 \times 10^{-3} - 3m^2T^2 \times 10^{-7}\end{aligned} \tag{3.22}$$

During electrolysis, bubbles are generated and flow in the electrolyte on which they reduce its conductivity. This phenomenon impacts the overall efficiency, and the corrected electrolyte conductivity is described by Bruggeman equation [19] [21], represented in Equation (3.23):

$$\sigma_{KOH-bubble} = \left(1 - \frac{2}{3}\theta\right)^{\frac{3}{2}} \sigma_{KOH} \tag{3.23}$$

This can also be translated in an electrolyte resistance considering the effect of bubbles as the following Equation (3.24):

$$R_{KOH-bubble} = R_{ele}\left(1 - \frac{2}{3}\theta\right)^{-\frac{3}{2}} \tag{3.24}$$

The membrane resistance R_{mem} is influenced by factors such as the membrane's porosity, tortuosity, cross-sectional area, and the conductivity of the electrolyte. For the inorganic Zirfon-based membrane used in the stack, R_{mem} is calculated by Equation (3.25):

$$R_{mem} = \frac{\delta_m \tau_m}{\varphi \sigma_{KOH} S_m} \tag{3.25}$$

where δ_m is the membrane thickness, τ_m is the membrane tortuosity, φ is the membrane porosity, and S_m is the cross-sectional area of the transverse membrane. AWE Voltage Model parameters are summarized in Table 3.4.

Table 3.4 – AWE Voltage Model parameters

Constant	Value	Units	Constant	Value	Units
$\mathcal{R}$	8.314	J·mol^{-1}·K^{-1}	δ_c	0.2	mm
p	1×10^5	Pa	S_a	0.42	m^2
F	9.65×10^4	C·mol^{-1}	d_a	2	mm
ω	0.32	-	d_c	2	mm
T_0	298.15	K	δ_m	0.5	mm
j_{lim}	300	kA·m^{-2}	τ_m	5.2	-
p_0	1×10^5	Pa	φ	0.59	-
δ_a	0.2	mm	S_m	0.42	m^2
S_a	0.42	m^2			

3.3. PEM Model

Building on the approach used for the AWE electrolyzer, the next step involves modelling the electrochemical behaviour of a single PEM cell. Although the technology differs in design and materials, the same fundamental equation is used to calculate the cell voltage U_{cell}, as shown in Equation (3.26). This expression includes the reversible voltage, activation overpotentials, and ohmic losses, capturing the key thermodynamic and kinetic phenomena that govern PEM electrolysis. While some secondary effects, such as mass transport limitations, may also play a role, they were omitted here to maintain consistency with the alkaline model and to keep the scope of the study focused and manageable.

$$U_{cell} = U_{rev} + U_{act,a} + U_{act,c} + U_{ohm} \tag{3.26}$$

For clarity and consistency, the main equations are presented again below, though definitions of commonly used terms are not repeated unless specific to this system.

3.3.1. Reversible Voltage

As in the alkaline model, the reversible voltage U_{rev} defines the minimum theoretical potential required for electrolysis and is calculated using the Nernst equation (3.27) [22]. The standard reversible voltage U_{rev}^{0} is used as reference point under standard conditions, as represented in Equation (3.28) [22]:

$$U_{rev} = U_{rev}^{0} + \frac{\mathcal{R}T}{2F} \ln\left[\frac{p_{H_2}\sqrt{p_{O_2}}}{p_{H_2O}}\right] \tag{3.27}$$

$$U_{rev}^{0} = 1.229 - 0.9 \times 10^{-3}(T - 298) \tag{3.28}$$

3.3.2. Activation Overpotential

In this model, the electrode current densities $j_{0,k}$, with $k = a$ for the anode and $k = c$ for the cathode, reflect the characteristics of PEM electrolysis and are defined by Equations (3.29) and (3.30), accordingly [22]:

$$U_{act,k} = \frac{\mathcal{R}T}{\alpha_k F} \operatorname{arcsinh}\left[\frac{j}{2j_{0,k}}\right] \tag{3.29}$$

$$j_{0,k} = j_{0,k-ref} \exp\left[-\frac{E_{act,k}}{\mathcal{R}}\left(\frac{1}{T} - \frac{1}{T_0}\right)\right] \tag{3.30}$$

where $j_{0,k-ref}$ is the reference electrode exchange current density at temperature T_{ref}, and $E_{act,k}$ is the activation energy for the water electrolysis reaction at the electrode.

3.3.3. Ohmic Overpotential

As previously discussed in the alkaline model, the passage of current through the cell components results in ohmic losses due to ionic and electronic resistances. In the PEM electrolyzer, these losses similarly contribute to a voltage drop that increases linearly with current density, as expressed by the following Equation (3.31) [22]:

$$U_{ohm} = R_{ion} \times j \tag{3.31}$$

In PEM electrolyzers, ohmic overvoltage comprises ionic and electronic components. However, due to the much lower conductivity of the membrane compared to the electronic parts, the ionic overvoltage dominates. Therefore, as in many models [20], [34], [35], the electronic contribution is neglected for simplicity. Given the short and uniform ionic path, membrane resistance is modelled using constant resistivity and is given by Equation (3.32) [22]:

$$R_{ion} = \frac{\delta_m}{\sigma_m} \tag{3.32}$$

where δ_m is the membrane thickness and σ_m is its ionic conductivity.

The membrane's ionic conductivity σ_m depends on both temperature and water content, and is calculated using the membrane water content λ_m as shown in Equation (3.33) [22]:

$$\sigma_m = (0.514\lambda_m - 0.326)\exp\left[1268\left(\frac{1}{303} - \frac{1}{T}\right)\right] \tag{3.33}$$

The membrane water content λ_m is modelled as a linear function of temperature, as shown in Equation (3.34) [22][23]:

$$\lambda_m = 0.08533T - 6.77632 \tag{3.34}$$

PEM Voltage Model parameters are summarized in Table 3.5.

Table 3.5 - PEM Voltage Model parameters

Constant	Value	Units	Constant	Value	Units
$\boldsymbol{p_{H_2}}$	1×10^5	Pa	$\boldsymbol{j_{0,c-ref}}$	191	A·m^{-2}
$\boldsymbol{p_{O_2}}$	0.21×10^5	Pa	$\boldsymbol{E_{act,a}}$	53.99×10^3	J·mol^{-1}
$\boldsymbol{p_{H_2O}}$	1×10^5	Pa	$\boldsymbol{E_{act,c}}$	53.99×10^3	J·mol^{-1}
$\boldsymbol{\alpha_a}$	2.47	-	$\boldsymbol{T_0}$	298.15	K
$\boldsymbol{\alpha_c}$	0.93	-	$\boldsymbol{\delta_m}$	0.254	mm
$\boldsymbol{j_{0,a-ref}}$	2×10^{-4}	A·m^{-2}			

3.4. Hydrogen Production

An essential outcome of electrolyzer operation is the quantification of hydrogen production, which is directly related to the input current and system efficiency. The molar flow rate of hydrogen $\dot{n}_{H_2}$ is given by Equation (3.35) [19]:

$$\dot{n}_{H_2} = \eta_F \frac{I}{zF} N_{cell} \tag{3.35}$$

where η_F is the Faraday efficiency, z is the number of electrons transferred per mole of hydrogen, and N_{cell} is the number of cells in the stack.

Faraday efficiency η_F is described as the following Equation (3.36) [19]:

$$\eta_F = \frac{j^2}{(2.5(T - 273.15) + 50) + j^2}\left(1 - 6.25 \times 10^{-6}(T - 273.15)\right) \tag{3.36}$$

The corresponding mass flow rate $\dot{m}_{H_2}$ is calculated by Equation (3.37) [19]:

$$\dot{m}_{H_2} = M_{H_2}\, \dot{n}_{H_2} \tag{3.37}$$

where M_{H_2} represents the molar mass of hydrogen. These expressions are used to estimate the hydrogen output based on the operating current and system configuration. The Hydrogen production parameters are illustrated in Table 3.6.

Table 3.6 – Hydrogen Production parameters

Constant	Value	Units
z	2	-
M_{H_2}	2.02	g·mol^{-1}

3.5. Heat Model

Thermal modelling is an essential part of simulating both AWE and PEM electrolyzers, as heat produced during operation influences system performance and stability. Since both systems share similar thermal characteristics, mainly due to overpotentials, resistive losses, and overall structure, a unified heat model is applied.

The model considers heat generation during electrolysis and its dissipation through convection, radiation, and thermal exchange with a cooling water stream at ambient temperature. While parameters are adjusted to reflect the specifics of each system, the overall structure of the model remains the same, allowing for a consistent and simplified implementation.

The heat generated by the electrolyzer during operation is calculated using the following Equation (3.38), which accounts for the electrical losses contributing to thermal energy [19]:

$$Q_{ele} = (U_{cell} - U_{th}) N_{cell} I \tag{3.38}$$

where U_{th} is the thermoneutral voltage.

The thermoneutral voltage U_{th} represents the voltage at which no net heat is produced or consumed during electrolysis, all the energy required for the reaction is supplied electrically and equals the enthalpy change ΔH of the reaction, as illustrated in Equation (3.39) [22].

$$U_{th} = \frac{\Delta H}{2F} \tag{3.39}$$

The following Equation (3.40) represents the enthalpy change for the water electrolysis reaction [22]:

$$\Delta H = \Delta H_{H_2} + \frac{1}{2}\Delta H_{O_2} - \Delta H_{H_2O} \tag{3.40}$$

where ΔH_{H_2} is the hydrogen enthalpy change, ΔH_{O_2} is the oxygen enthalpy change, and ΔH_{H_2O} is the water enthalpy change.

The enthalpy change for each component i can be described as the difference between the actual state and the reference state, as shown in Equation (3.41):

$$\Delta H_i = \Delta H_i(T) - \Delta H_i(T_0) \tag{3.41}$$

The total heat loss from the electrolyzer stack to the environment is expressed by Equation (3.42) as the sum of the heat loss mechanisms, convection Q_{conv} and radiation Q_{rad} [24]:

$$Q_{loss} = Q_{conv} + Q_{rad} = h\, A_{stack}(T - T_{amb}) + \sigma\, A_{stack}\, \varepsilon_{stack}\left(T^4 - {T_{amb}}^4\right) \tag{3.42}$$

where h is the convective heat transfer coefficient, A_{stack} is the external surface area of the stack, T is the stack temperature, T_{amb} is the ambient temperature, σ is the Stefan-Boltzmann constant, and ε_{stack} is the surface emissivity of the stack.

The thermal behaviour of the electrolyzer also depends on the heat exchanged with the cooling water, which absorbs part of the generated heat to maintain system temperature. This heat exchange is directly related to the enthalpy change of the water involved in the reaction. The enthalpy of water, ΔH_{H_2O}, varies with temperature and can be approximated by the Equation (3.43) [25]:

$$\Delta H_{H_2O} = \Delta H^0_{H_2O} + 72.39(T - T_0) + 4.69 \times 10^{-3}(T^2 - T_0^2) \tag{3.43}$$

where $\Delta H^0_{H_2O}$ is the reference water enthalpy at temperature T_0, and T is the operating temperature. This temperature-dependent enthalpy allows accurate modelling of the heat absorbed or released by the cooling water during electrolysis, which is essential for the system's thermal management.

The heat absorbed or released by the cooling water during electrolysis can be calculated using the following Equation (3.44) [25]:

$$\Delta Q_{H_2O} = \frac{q \rho_{H_2O}}{M_{H_2O}} \left(\Delta H^{in}_{H_2O} - \Delta H^{cell}_{H_2O}(-0.0077(T - T_0) + 1)\right) \tag{3.44}$$

where q is the volumetric flow rate of cooling water, ρ_{H_2O} is the density of water, M_{H_2O} is the molar mass of water, and $\Delta H^{in}_{H_2O}$ and $\Delta H^{cell}_{H_2O}$ are the enthalpies of the water at the inlet and at the electrolyzer cell temperature, respectively. The corrective heat model used in Equation (3.44) of the referenced study introduces a temperature-dependent correction factor to enhance the model's accuracy, $(-0.0077(T - T_0) + 1)$, which is applied solely to the enthalpy term $H^{cell}_{H_2O}$. However, upon closer inspection and comparison with calculated

values, it was found that this formulation results in significant inaccuracies in heat flow estimation.

Specifically, the correction factor should be applied to the enthalpy difference $\left(\Delta H_{H_2O}^{in} - \Delta H_{H_2O}^{cell}\right)$, rather than to the cell enthalpy term alone. This discrepancy can lead to misrepresentation of the temperature-driven variation in thermal energy transfer. Therefore, the corrected form of the previous Equation (3.44) is proposed as Equation (3.45):

$$\Delta Q_{H_2O} = \frac{q\rho_{H_2O}}{M_{H_2O}}\left(\Delta H_{H_2O}^{in} - \Delta H_{H_2O}^{cell}\right)(-0.0077(T - T_0) + 1) \tag{3.45}$$

This correction ensures that the thermal model reflects the actual energy exchange driven by the enthalpy difference between the inlet water and the cell conditions, thereby improving the accuracy of dynamic simulations.

Table 3.7 presents the Heat Model parameters.

Table 3.7 - Heat Model parameters

Constant	Value	Units
$\Delta \boldsymbol{H_{H_2}}$	0	J·mol^{-1}
$\Delta \boldsymbol{H_{O_2}}$	0	J·mol^{-1}
$\boldsymbol{T_{amb}}$	298.15	K
$\boldsymbol{\sigma}$	5.67× 10^{-8}	J·K^{-1}
$\boldsymbol{\varepsilon_{stack}}$	0.8	-

Constant	Value	Units
$\Delta \boldsymbol{H^0_{H_2O}}$	-2.86 × 10^5	J·mol^{-1}
$\boldsymbol{T_0}$	298.15	K
$\boldsymbol{\rho_{H_2O}}$	1	g·cm^{-3}
$\boldsymbol{M_{H_2O}}$	18.02	g·mol^{-1}

The overall thermal behaviour of the electrolyzer cell is described by the heat transfer balance, which accounts for the electrical heat generation, heat exchanged with the cooling water, and heat losses to the environment. This balance is expressed as in Equation (3.46):

$$C\frac{dT}{dt} = Q_{ele} + \Delta Q_{H_2O} - Q_{loss} \tag{3.46}$$

where C is the thermal capacity of the cell.

This equation captures the dynamic temperature response of the cell under varying operating conditions.

The parameters h and C were estimated so that the electrolyzer takes 1 hour to heat up from room temperature to its nominal temperature while operating at full power and 5 hours to cool down back to the room temperature plus 10% of the difference between nominal and room temperatures through convection and radiation. It is important to mention

that a simulation was conducted for each model due to their differences. The following parameters are detailed in Table 3.8.

Table 3.8 – Estimated heat transfer coefficients

	Constant	Value	Units		Constant	Value	Units
AWE	$\boldsymbol{h}$	99.3	$W \cdot m^{-2} \cdot K^{-1}$	**PEM**	$\boldsymbol{h}$	306.2	$W \cdot m^{-2} \cdot K^{-1}$
	$\boldsymbol{C}$	30.7	$MJ \cdot K^{-1}$		$\boldsymbol{C}$	10.9	$MJ \cdot K^{-1}$

3.6. Power Acquisition

The values of renewable energy, solar power P_{solar} and wind power P_{wind}, were retrieved from REN's DataHub [26] for April and May of 2025. These values were manipulated to consider a 2 MW hybrid solar-wind park for these electrolyzers by calculating the power relative to its maximum from the DataHub data. The values were then stored in text files, containing the nominal power for each 15 minutes.

3.7. Optimization Problem

The main goal of this work is to maximize the profit over time by adjusting the current and the cooling water rate. To create a more realistic scenario, a restriction for the daily hydrogen production was also created, which ensures that the minimum daily production should be at least 1/3 of the maximum daily production allowed for each electrolyzer. The optimization problem was formulated using CasADi as the following Equations (3.47) to (3.51):

$$J = \int_0^{t_f} \left(-\dot{m}_{H_2} \, Price_{H_2} - P_{grid} \frac{Price_{grid}}{3600} \right) dt \tag{3.47}$$

$$T_{amb} \leq T(t) \leq T_{nom} \tag{3.48}$$

$$0 \leq I \leq A_{cell} j_d \tag{3.49}$$

$$0 \leq q \leq q_{max} \tag{3.50}$$

$$\int_0^{t_{day}} \dot{m}_{H_2} dt \geq \beta DailyMax_{H_2} \tag{3.51}$$

where J is the cost minimized by the solver, which is symmetrical to the accumulated profit in euros (€), $Price_{H_2}$ is the hydrogen price ($€ \cdot kg^{-1}$) which was considered constant and equal to 2 $€ \cdot kg^{-1}$, an optimistic value for future years, $Price_{grid}$ is the grid power price ($€ \cdot MWh^{-1}$) retrieved from REN's DataHub like solar and wind power, T_{nom} is the nominal temperature of the electrolyzer, t_f is the operation time in seconds (s), j_d is the maximum current density ($A \cdot m^{-2}$), q_{max} is the maximum estimated water flowrate for the optimal hydrogen production

($cm^3 \cdot s^{-1}$), β is a dimensionless parameter set to 1/3 to represent the daily demand of hydrogen, $DailyMax_{H_2}$ is the maximum daily production possible for the electrolyzer (kg), and t_{day} is the time of a day in seconds (s). The objective function and constraint parameters common to both models are detailed in Table 3.9, while the parameters specific to each model are presented in Table 3.10.

Table 3.9 – Objective function and constraints parameters

Constant	Value	Units
$\boldsymbol{Price_{H_2}}$	2	€·kg^{-1}
$\boldsymbol{T_{amb}}$	298.15	K
$\boldsymbol{T_{nom}}$	333.15	K

Table 3.10 – Constraints parameters for each model

	Constant	Value	Units		Constant	Value	Units
AWE	$\boldsymbol{j_d}$	5000	A·m^{-2}	**PEM**	$\boldsymbol{j_d}$	10000	A·m^{-2}
	$\boldsymbol{q_{max}}$	1852.3	$cm^3 \cdot s^{-1}$		$\boldsymbol{q_{max}}$	336.6	$cm^3 \cdot s^{-1}$
	$\boldsymbol{DailyMax_{H_2}}$	414	kg		$\boldsymbol{DailyMax_{H_2}}$	600	kg

Regarding the activation overpotential, it represents the energy barrier that must be overcome to initiate electron transfer at the electrode. This phenomenon is captured quantitatively by the Butler–Volmer equation (3.52), which relates the overpotential to the current density, accounting for both anodic and cathodic reactions [27].

$$j = j_0 \left[\exp\left(\frac{\alpha_a 2F}{\mathcal{R}T}\eta\right) - \exp\left(\frac{\alpha_c 2F}{\mathcal{R}T}\eta\right) \right] \tag{3.52}$$

This equation has two limiting cases: a lower overpotential region, namely called polarization resistance, where the overpotential value is very close to 0, and high overpotential region. The Butler-Volmer equation can be approximated to Tafel equation (3.53), and it can be rewritten to obtain the overpotential as a function of the current, as follows [28]:

$$\eta = \frac{\alpha \mathcal{R}T}{2F} \ln\left(\frac{j}{j_0}\right) \tag{3.53}$$

Alternatively, its variation can be expressed in terms of the inverse hyperbolic sine function, as shown in Equation (3.54) [27]:

$$\eta = \frac{\mathcal{R}T}{2F}\sinh^{-1}\left(\frac{j}{2j_0}\right) \tag{3.54}$$

But at lower overpotentials, when $\eta \approx 0$, namely the polarization resistance region, the linear term of the equation dominates, and linearity can be assumed. So, when the current is small enough, resulting in overpotentials lower than 15 mV, the Butler-Volmer equation is approximated as a linear relation between j and η [27].

To simplify the implementation of the Butler–Volmer equation in computational frameworks such as Python, the original logarithmic expression of the overpotential dependence was reformulated using the inverse hyperbolic sine function. While the classical form includes a natural logarithm that can lead to negative arguments under certain current density conditions, requiring conditional logic to handle positive and negative branches, the $\sinh^{-1}$ formulation provides a mathematically similar but computationally smoother alternative. This transformation avoids the need for explicit branch handling, improves numerical stability, and allows for a more straightforward evaluation across the entire current density range. As such, the overpotential expression for AWE was rewritten using the inverse hyperbolic sine to maintain accuracy while enhancing implementation simplicity, as represented in Equation (3.55):

$$U_{act,k} = \frac{\mathcal{R}T}{2\alpha_k F}\sinh^{-1}\left[\frac{j}{2j_{0,k}(1-\theta)}\right] \tag{3.55}$$

As previously mentioned, several simplifications were made to the system to simplify the model and due to the restrictive time of the dissertation. In the models, not all possible overpotential losses were considered, such as concentration, electrode contamination, membrane, and electrodes deterioration. Additionally, it is assumed that the system can change the current instantaneously. Although this simplification introduces a potential safety risk, since a sudden increase in current can cause the generation of explosive gas mixtures and impose mechanical stress on the electrolyzer materials, it is not expected to significantly impact the optimization results. This is because, in practice, current transitions typically occur over a timescale of several seconds, allowing the system to settle into new operating conditions without major deviations from the model assumptions [29]. The grid price was assumed equal either buying or selling. All hydrogen is sold to the grid, avoiding storage and transport potential outcomes. The temperature and heat parameters, convection coefficient and thermal capacity, are constant throughout the electrolyzer to ensure uniformity of the values. Startup and shutdown times and minimum power were not considered, which is a limitation that affects the results since these technologies have power loadout restrictions and these times can range from 30 to 60 minutes [30]. In this model, it is assumed that the entire water feed to the electrolyzer exceeds the stoichiometric

requirement for hydrogen production. This additional amount, referred to as excess water and through the model as cooling water, serves a dual purpose by acting as a coolant. It facilitates heat dissipation from the system and is therefore be referred to as cooling water. Additionally, it is assumed that a cooling tower of adequate capacity is available to maintain the water temperature constantly at 298.15 K. The renewable energy power used has no purchase cost associated as it is assumed that these electrolyzers are integrated into an established 2 MW hybrid solar-wind facility, with each renewable energy technology (solar and wind) contributing 1 MW of production capacity. Also, this optimization problem does not consider any costs associated to external equipment/raw materials, such as fans/air conducts to achieve the desired convection heat transfer coefficient, water price as electrolysis raw material and heat exchanger, pipes, water pumps, and any other relevant cost which could be associated to this plant, namely electrolyzer equipment cost, installation, transport, operation, and maintenance costs.

4. Results and discussion

By applying the models created with the data extracted from REN DataHub for daily production of renewable energy power and daily grid power price, 3 different simulations were run: a base scenario to gather relevant data and conclusions about the model and two comparative scenarios with strict data selection to input in the models.

For a first analysis, a 4-day period was evaluated in the model. As previously mentioned, the price is updated hourly and the renewable energy power in 15-minute intervals, and these data correspond to 20-24 of April 2025. The current trajectory is presented in Figure 4.1 for the AWE model and Figure 4.2 for the PEM model. Further graphical representations illustrating relevant variable data, such as cooling water flow rate, temperature, hydrogen production, voltage, and renewable power histories can be found in Appendix A for both models.

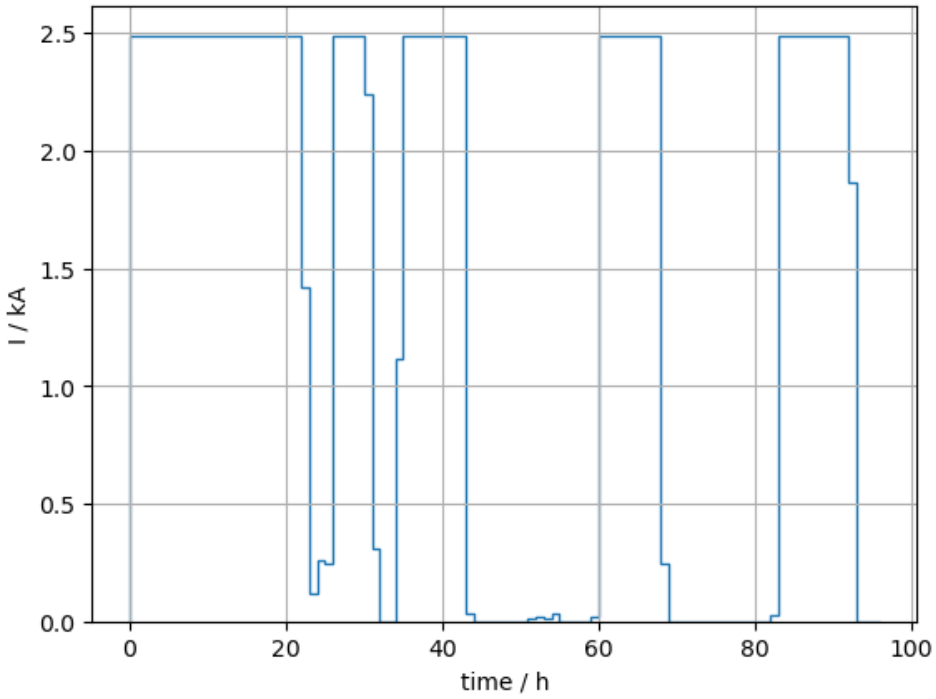

Figure 4.1 – Current trajectory obtained by CasADi for the AWE model

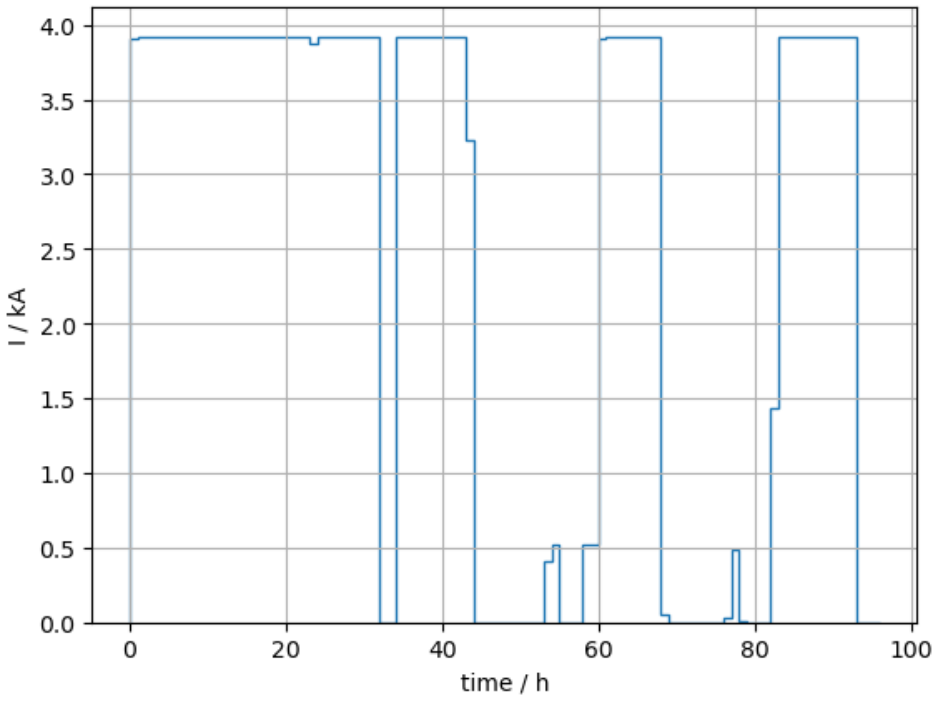

Figure 4.2 - Current trajectory obtained by CasADi for the PEM model

The objective function tends to maximize the hydrogen production via manipulation of the input variables of the system, current and cooling water. An important factor in play is the integration of grid power with the system to increase the power in times where it is economically advantageous to produce hydrogen and when the renewable energy source does not fully provide the required power. So, when it is economically advantageous to produce hydrogen, the optimizer increases the current, consequently leading to temperature rising as the electrolysis reaction occurs. As the system approaches the nominal temperature, where hydrogen production is at its highest, the optimizer adjusts the cooling water flow to maintain thermal stability. Maintaining the nominal temperature is important not only for maximizing production but also for ensuring system safety, preserving component lifespan and maintaining electrolyte stability.

On the other hand, when it is not economical viable to produce hydrogen, the optimizer reduces the current. This action causes a gradual temperature decrease, and the cooling water is not necessary. As a consequence of the current decrease, the electrolyzer power also diminishes and the energy surplus from solar and wind power is sold directly to the public electric grid. Engaging in a comprehensive examination of major economic determinants, the relevant data were presented in a unified graphic format to facilitate both quantitative and qualitative analysis.

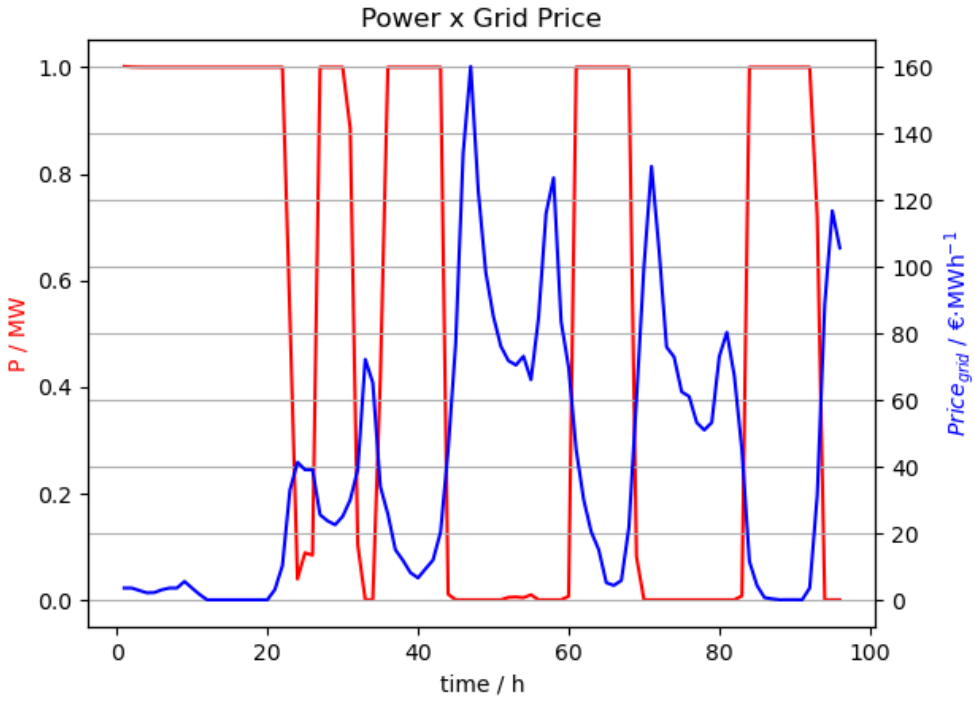

Figure 4.3 - Electrolyzer power consumption and grid prices histories obtained by CasADi for the AWE model

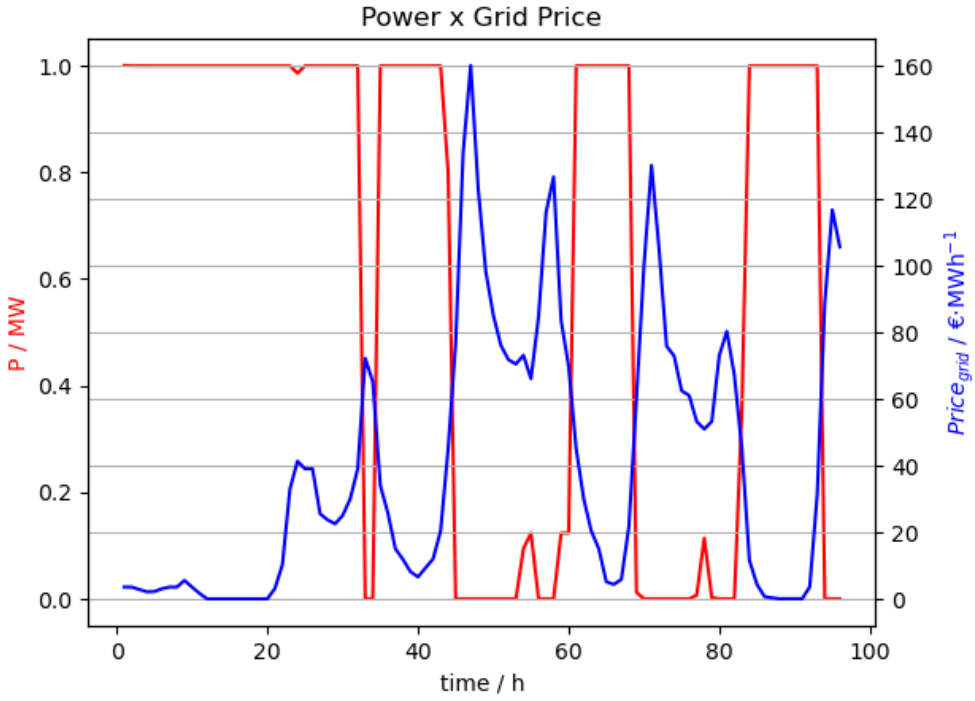

Figure 4.4 - Electrolyzer power consumption and grid prices histories obtained by CasADi for the PEM model

Even though AWE and PEM operate differently, both models follow the same optimization principle, as shown in Figures 4.3 and 4.4, respectively. The optimization framework establishes a strategic electricity price threshold, above which selling renewable

energy to the grid is economically advantageous, and below which utilizing it for hydrogen production is more cost-effective.

This behaviour is illustrated in Figures 4.3 and 4.4. For the AWE model (Figure 4.3), during high-price periods such as the 34-hour peak, 45–60 hours and 70-85 hours, the electrolyzer is turned off or operates at minimal power, with all available electricity sold to the grid. The PEM model (Figure 4.4) exhibits similar behaviour at the same time ranges. However, PEM is still able to partially operate (~0.12 MW) at the 54 and 77-hour marks. This is due to PEM's higher hydrogen production capacity, which leads to a higher strategic electricity grid price, compared to AWE, making it worthwhile to continue hydrogen production even at high electricity prices. Interestingly, at the 25-hour mark, PEM opts to purchase electricity to maintain a high electrolyzer load (~0.99 MW), while AWE is close to a complete shut down and sells the remaining power to the grid, as illustrated in Figure A.10. This divergence underscores PEM's operational flexibility and efficiency and its higher strategic electricity grid price, allowing it to remain active when AWE does not.

Overall, both models react similarly to price peaks, especially at 45 hours, but evaluate subsequent peaks differently based on their performance characteristics. When prices are lower than the strategic threshold, at 0–33, 35-45, 60–68 and 84-92 hours, excluding the 45-hour spike, both models purchase electricity and operate the electrolyzers at maximum capacity. While grid prices largely dictate the power flow decisions, the optimizer also accounts for real-time performance and economic trade-offs, occasionally deviating from a strict price-driven strategy.

In the second simulation phase, a rolling optimization strategy was used, evaluating a four-day horizon within each 24-hour period. On day 1, the model optimized decisions for days 1–4; on day 2, the window shifted to days 2–5, and so on. This approach accounts for short-term uncertainties in grid prices. It was assumed that prices for the first two days were known, while days 3 and 4 were affected by pseudorandom uncertainties of ±5% and ±15%, respectively, drawn from a uniform distribution. To aid convergence, each day's uncertainty was applied uniformly, i.e., all prices on day 3 were scaled by the same random factor and likewise for day 4, reducing intra-day volatility, helping the solver avoid instability, and leading the optimizer algorithm to a feasible solution without cycling or crashing. This method simulates real-world price variability and evaluates its impact on the optimizer's decision-making. Two datasets were used for each model, representing different weeks in May 2025: a normal week scenario with moderate prices and an expensive week scenario with higher prices. Starting with the normal week results, the following Figures 4.5 and 4.7 and Figures 4.6 and 4.8 illustrate the real trajectory of the current and the current trajectory for the grid price uncertainty analysis, for AWE and PEM, respectively.

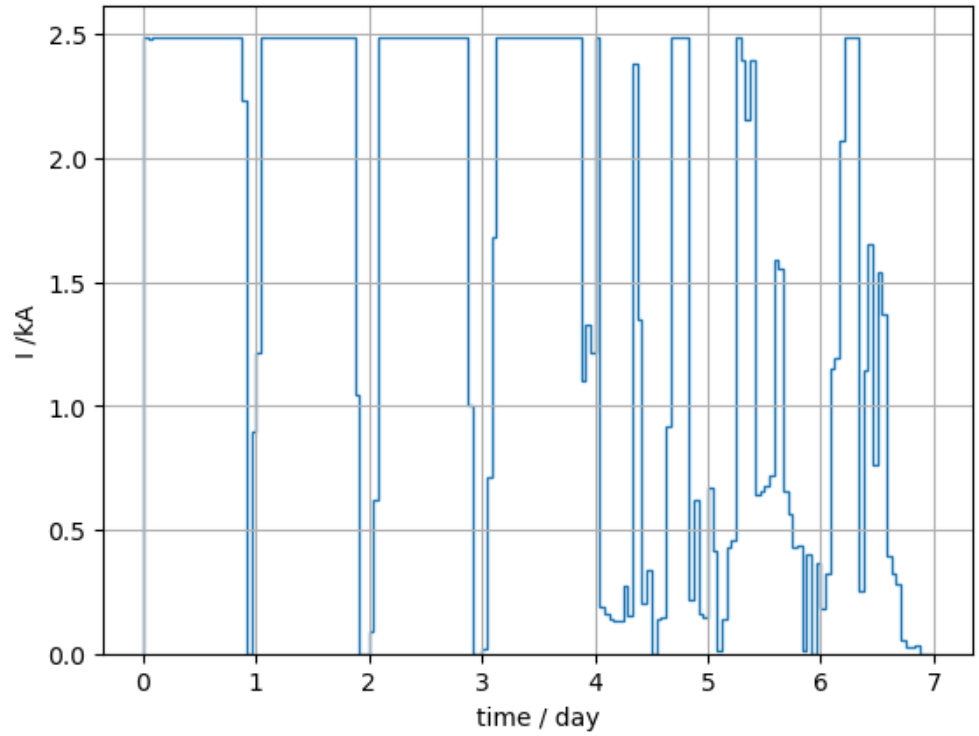

Figure 4.5 – Real trajectory obtained for the uncertainty analysis obtained by CasADi in the normal week for AWE

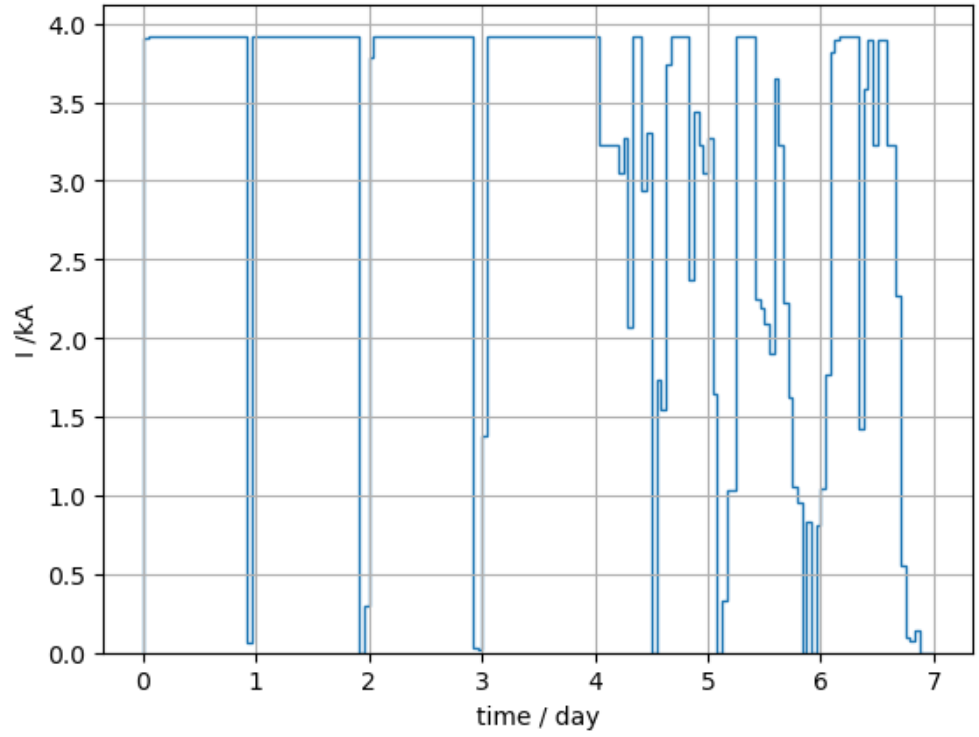

Figure 4.6 - Real trajectory obtained for the uncertainty analysis obtained by CasADi in the normal week for PEM

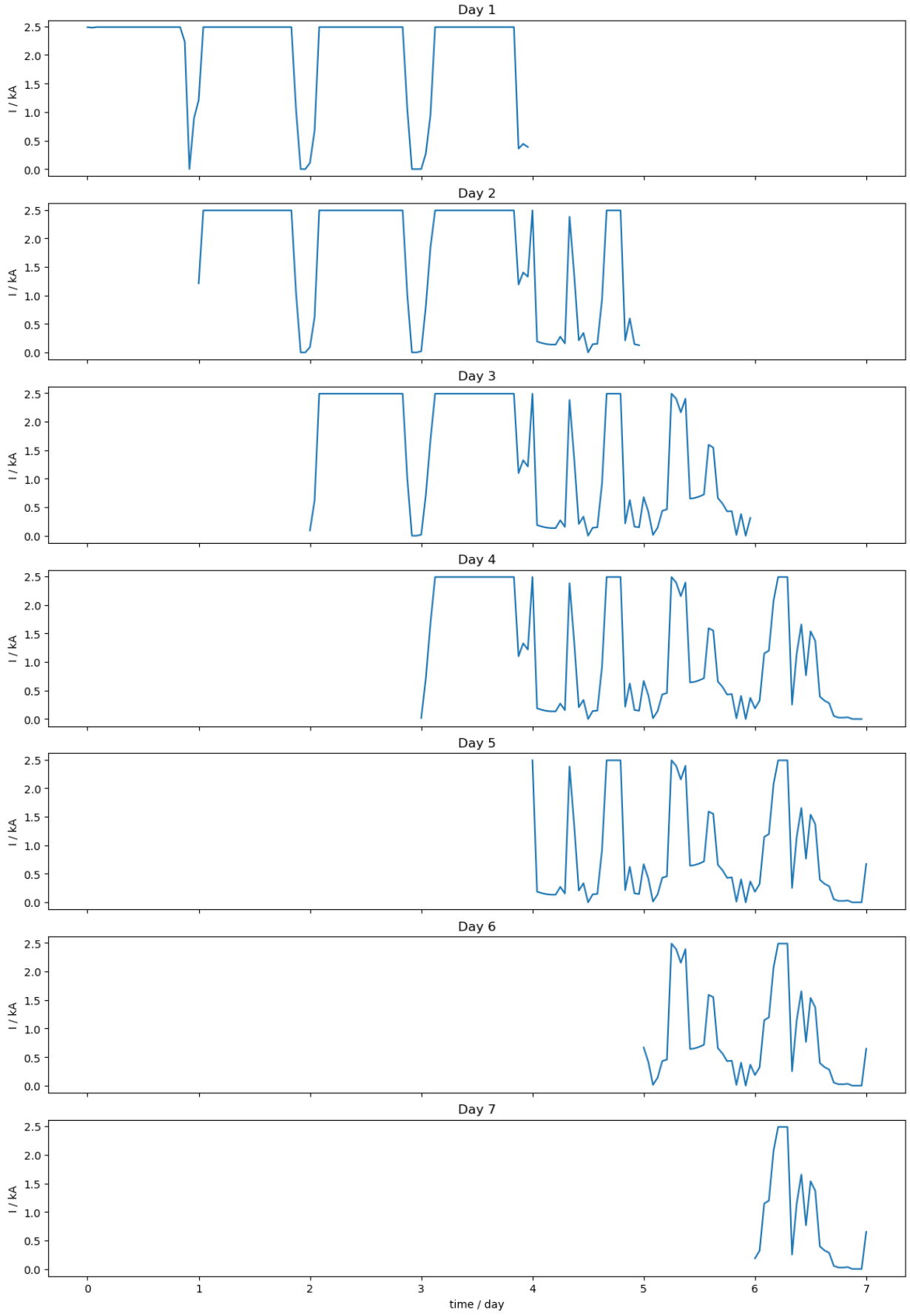

Figure 4.7 – Current trajectory with grid price uncertainty analysis obtained by CasADi in the normal week for AWE

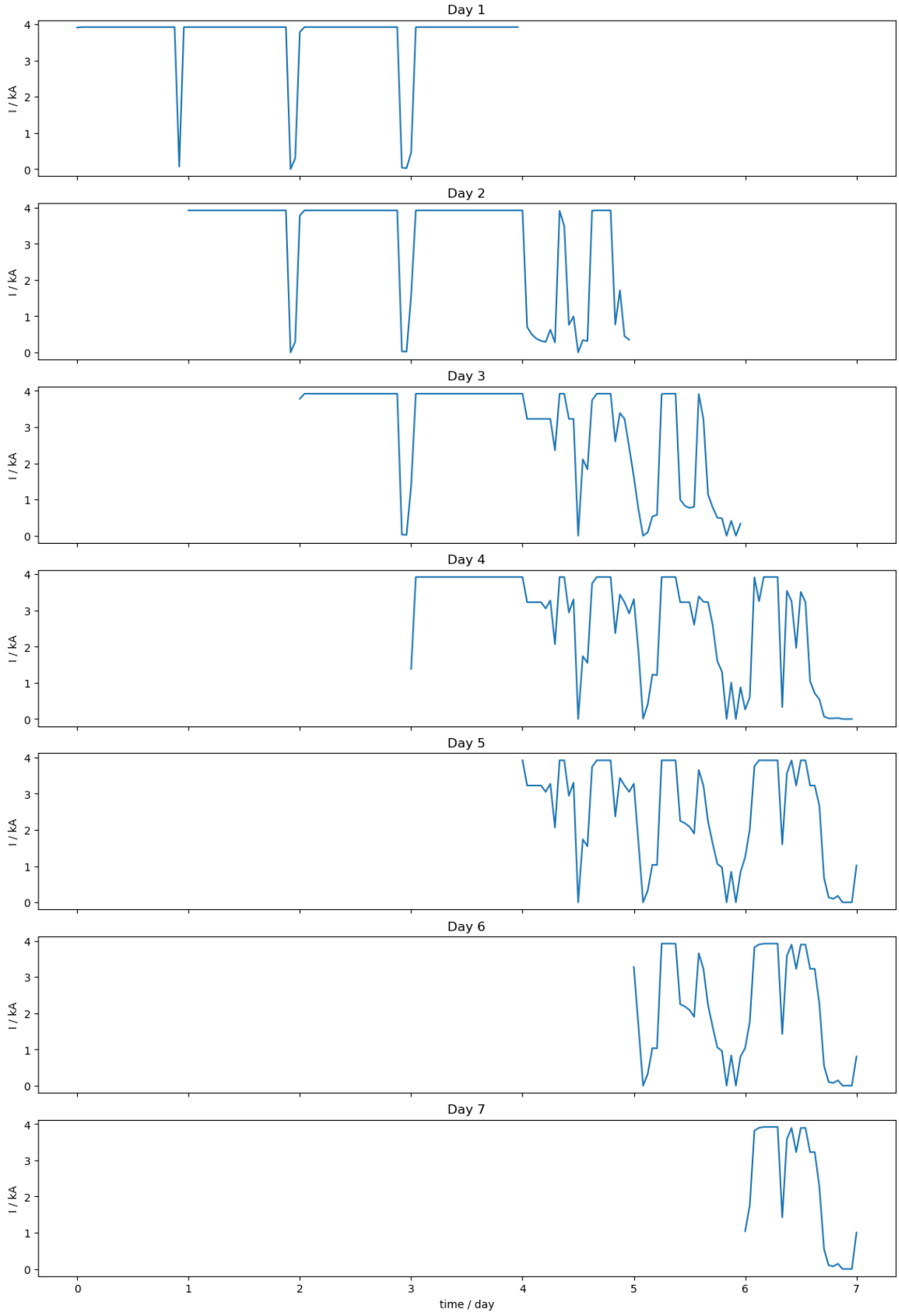

Figure 4.8 - Current trajectory with grid price uncertainty analysis obtained by CasADi in the normal week for PEM

As illustrated in Figure 4.7 and Figure 4.8, the introduction of price uncertainties leads to varying effects on the current trajectory in the AWE and PEM models, respectively. In some cases, the trajectory remains largely consistent, indicating limited sensitivity to small fluctuations. However, in other instances, noticeable deviations occur, suggesting that the optimizer's decisions can be influenced when the uncertainty aligns with more critical cost or timing conditions. These deviations are clearly noticeable on the PEM model. The deviation in current between Day 2 and Day 5, in Figure 4.8, reflects how the optimizer reacts to variations in grid electricity prices. While the hydrogen price remains fixed, the optimizer evaluates the strategic electricity grid price to dynamically assess whether it's more cost-effective to operate the system or keep it off regarding the economical signal input. These decisions differ slightly between simulation days due to the shifting four-day optimization window. Even when time periods overlap, notorious changes in future price uncertainty influence the outcome, leading to slight adjustments in operation from one day to the next. Among the two electrolyzer models studied, only this one showed noticeable deviations in operation due to price uncertainties. This behaviour is likely linked to its higher production capacity per hour. Since this electrolyzer can produce more hydrogen, the associated electricity costs have a greater impact on the optimization outcome. As a result, fluctuations in grid prices more strongly influence the decision to operate or remain idle compared to the smaller-capacity system.

Now for the expensive week scenario, the following Figures 4.9 and 4.11 and Figures 4.10 and 4.12 illustrate the grid price uncertainty analysis, real trajectory of the current and current for the uncertainty analysis, for AWE and PEM, respectively.

Since electricity prices remain consistently high in this scenario, minor fluctuations have a reduced influence on the optimizer's decisions, as shown in Figures 4.11 and 4.12. When prices are high, the incentive to adjust operations in response to small changes diminishes, leading to a more stable optimization strategy. As a result, deviations in current trajectories between simulation days are less pronounced, with operations reflecting the high-cost environment rather than reacting sensitively to small price uncertainties. In this context, the AWE model is more affected, as seen in the current deviations from Day 2 to Day 5 in Figure 4.11. Although less noticeable than in the PEM model during the normal week, the higher price variance here still impacts the electrolyzer's response, prompting a reduction in production, evident from the lower current peaks on the final day of each simulation (one of the two days subject to price variance). This indicates that AWE is more sensitive to high price scenarios, while PEM, though affected as shown in Figure 4.12, exhibits a more stable response.

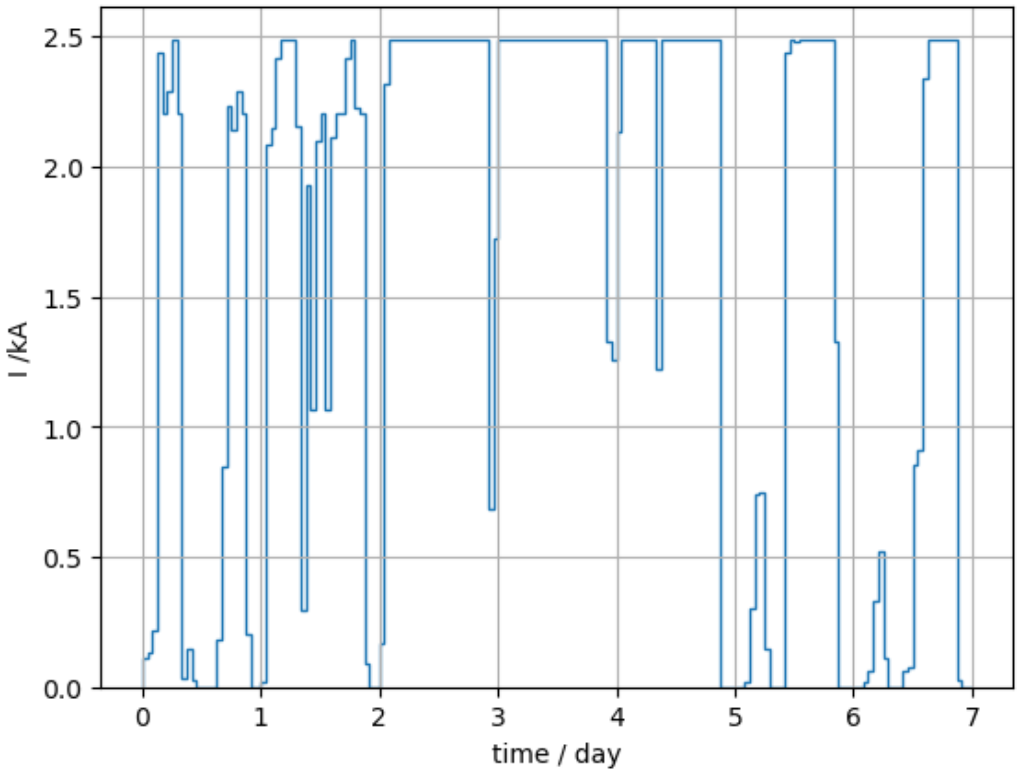

Figure 4.9 - Real trajectory obtained for the uncertainty analysis obtained by CasADi in the expensive week for AWE

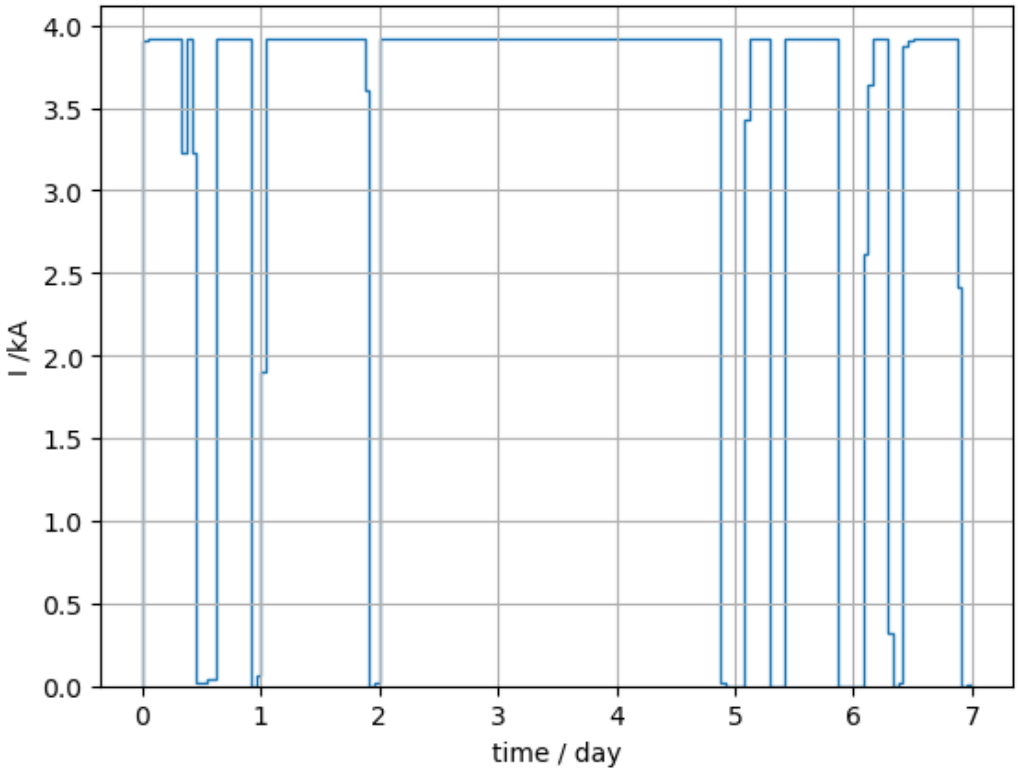

Figure 4.10 - Real trajectory obtained for the uncertainty analysis obtained by CasADi in the expensive week for PEM

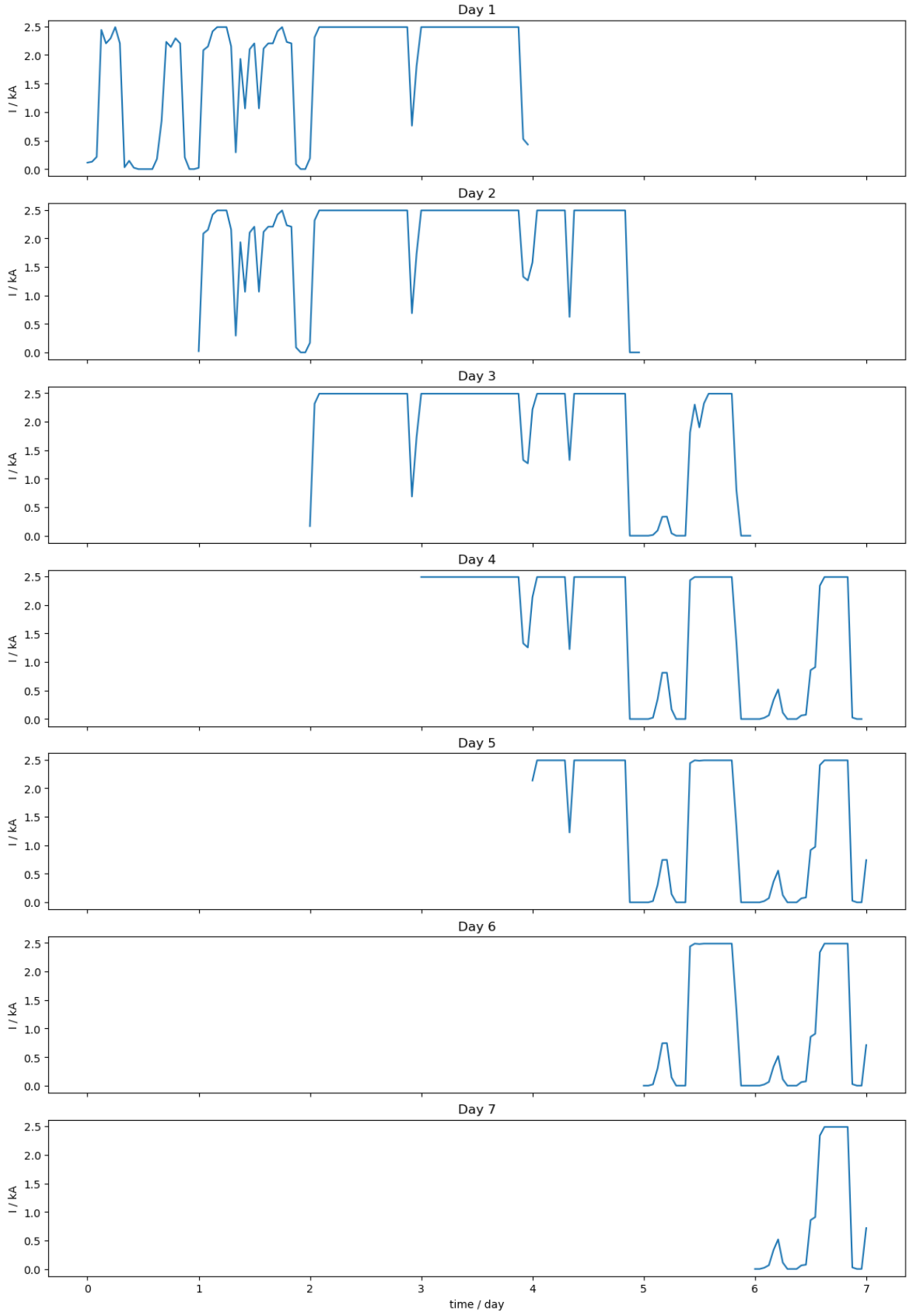

Figure 4.11 - Current trajectory with grid price uncertainty analysis obtained by CasADi in the expensive week for AWE

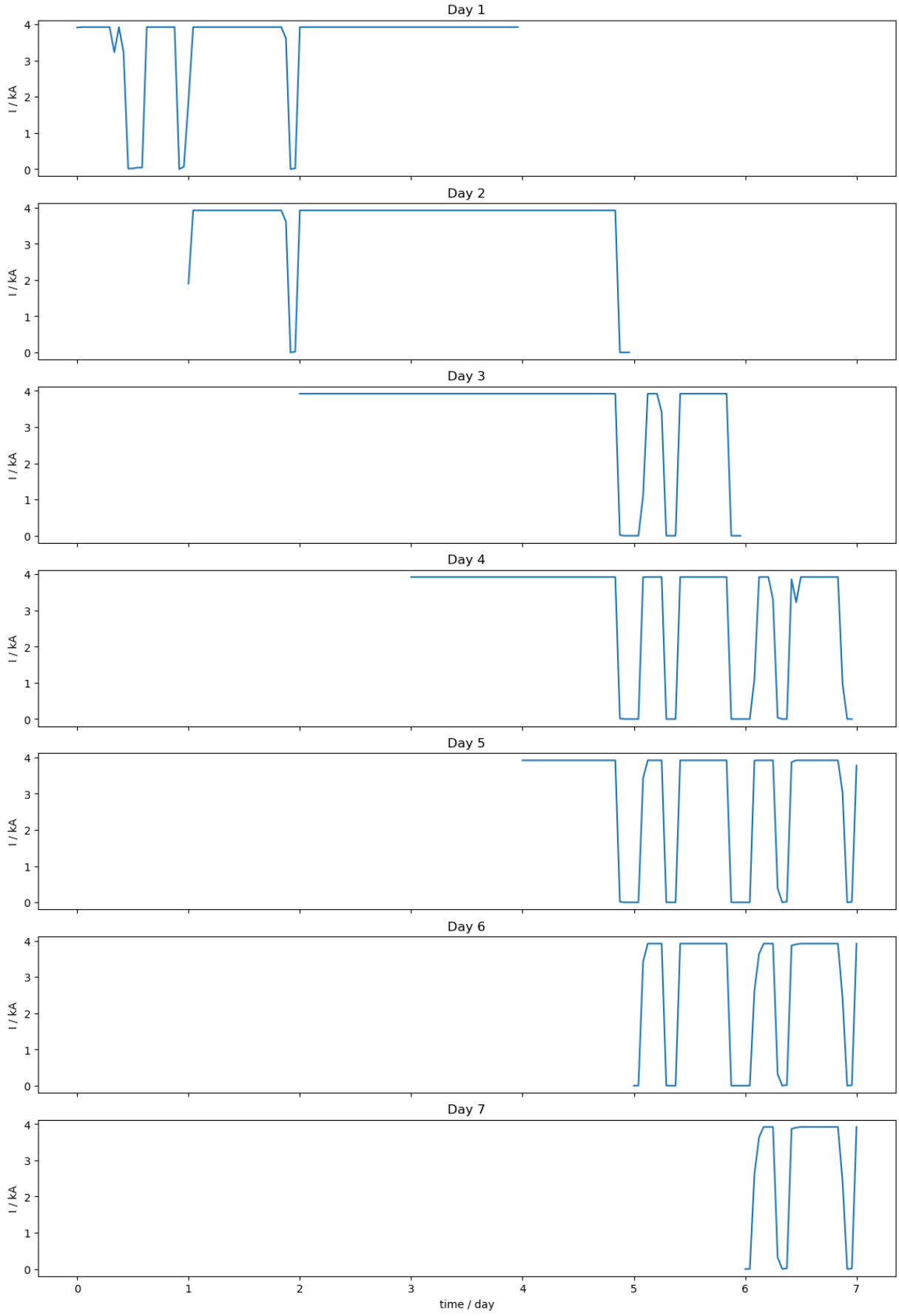

Figure 4.12 - Current trajectory with grid price uncertainty analysis obtained by CasADi in the expensive week for PEM

As observed during the normal week, smaller price deviations can significantly impact profitability. Under such conditions, the optimizer targets specific price points to determine whether electricity purchases are economically viable, making the system more sensitive to fluctuations and resulting in greater operational variation between days.

Despite differences in electricity prices and renewable inputs across the two weeks, the optimizer achieved comparable profits: for AWE, 4592€ in the normal week and 4512€ in the expensive week; for PEM, 6067€ and 6164€, respectively. While AWE's profit slightly decreased under higher electricity prices, PEM's profit marginally increased. This contrast highlights the different ways each system responds to market conditions. High electricity prices create more attractive opportunities to sell surplus renewable energy to the grid, while lower prices enable the optimizer to purchase electricity economically and increase hydrogen production. The PEM electrolyzer, with its higher production capacity, is better equipped to adapt to price fluctuations. Its greater flexibility allows the optimizer to selectively operate during economically favourable periods, even under high-cost scenarios. AWE's lower production capacity and reduced responsiveness make it more sensitive to price increases, leading to reduced operating hours and output. As result, its profit slightly declines in the expensive week. These outcomes illustrate the optimizer's ability to dynamically adjust strategies depending on the system characteristics and economic signals. These results highlight the influence of input variability and randomness on system performance. Rather than indicating a precise economic balance, they demonstrate the system's ability to adapt to changing conditions. The optimizer adjusts operational strategies, accordingly, leading to similar performance outcomes across scenarios. This suggests that, despite differing inputs, the model identifies robust solutions that maintain profitability and production within a consistent range.

To evaluate the system's response to the product price deviations, a hydrogen price reduction scenario was developed. This sensitivity analysis focused solely on the price reduction case. A scenario involving increasing hydrogen price was excluded, as it would likely result in both AWE and PEM systems operating continuously at nominal power, since higher hydrogen prices would consistently justify purchasing grid electricity. While technically valid, such a scenario does not yield meaningful insights aligned with the study's objectives. The following simulations also employed the rolling optimization strategy, under the same conditions and price variances as in the previous case.

The following Figure 4.13 and Figure 4.14 illustrates the grid price uncertainty analysis for the normal week with the new hydrogen price, 1.5 €·kg^{-1}, for AWE and PEM, respectively.

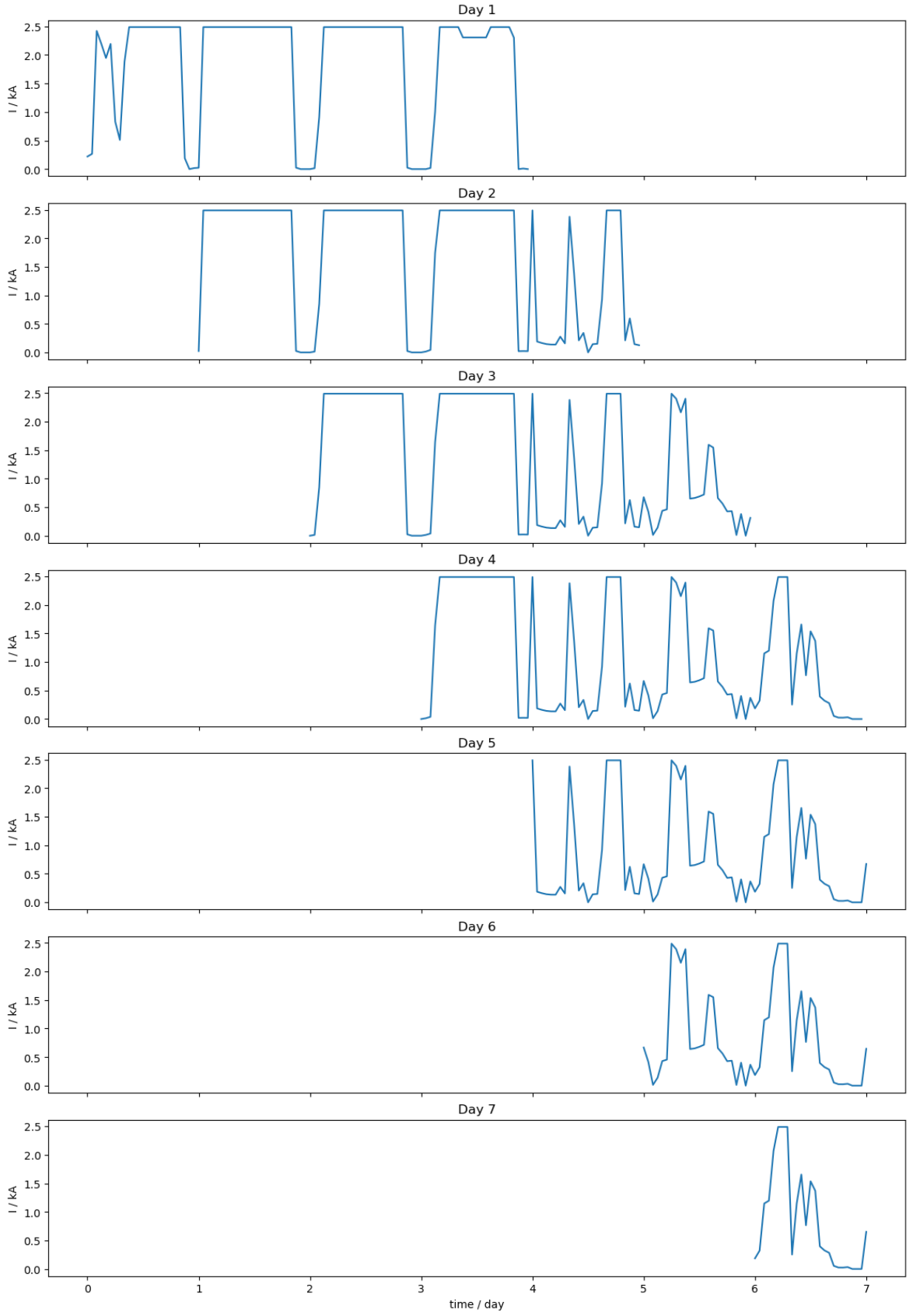

Figure 4.13 - Current trajectory with hydrogen price reduction and grid price uncertainty analysis obtained by CasADi in the normal week for AWE

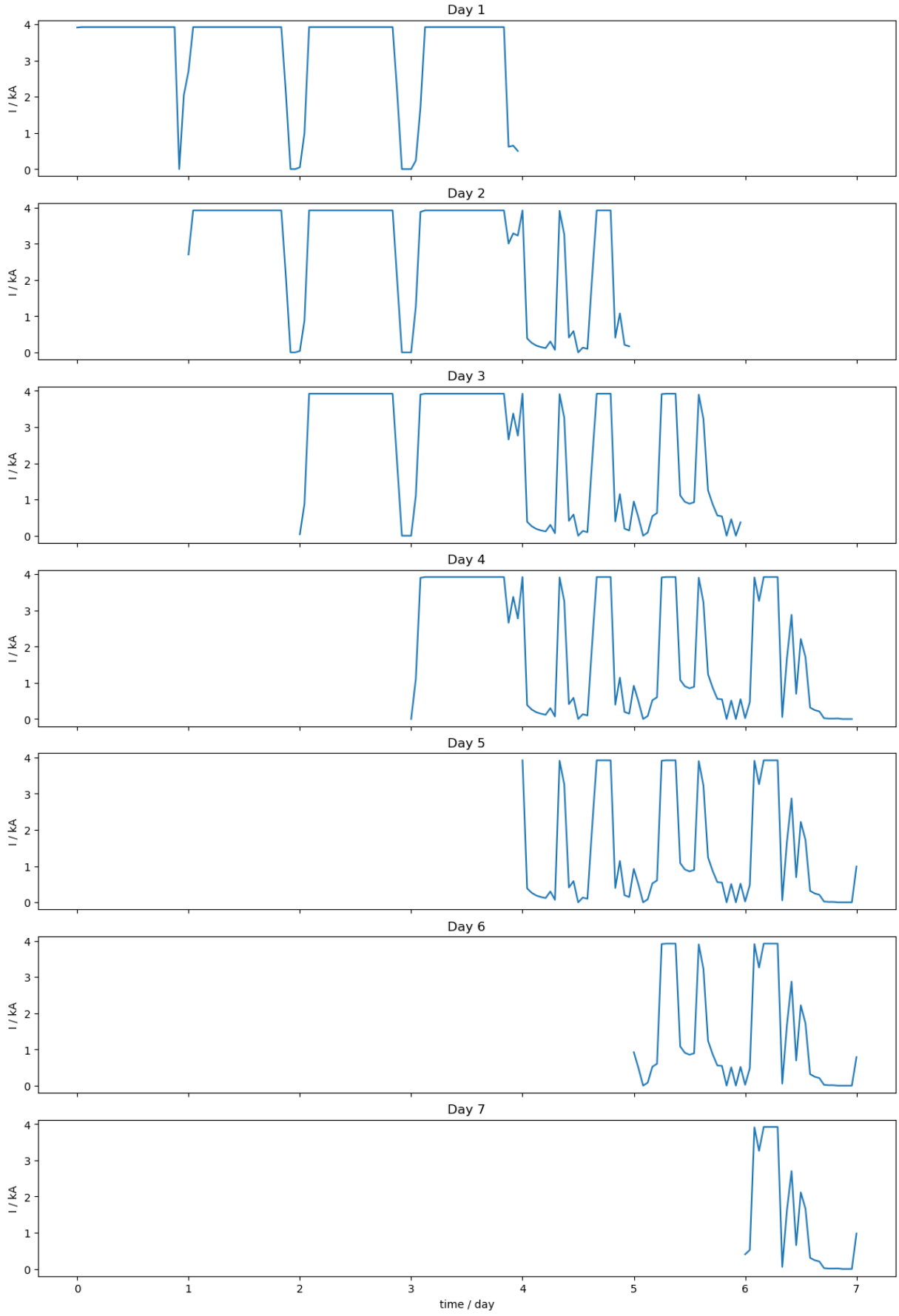

Figure 4.14 - Current trajectory with hydrogen price reduction and grid price uncertainty analysis obtained by CasADi in the normal week for PEM

The Figure 4.13 and Figure 4.14 clearly illustrate the importance of using the right price. This parameter, resulting in a lower strategic electricity grid price, leads the optimizer to make sharper and more extensive turn-off periods as shown between Day 1 and Day 4 in both models due to the less appealing hydrogen revenue. For the AWE model, Figure 4.13, in Day 5 to Day 7 no change is seen relative to the previous scenario. This phenomenon is justified by the daily production restriction imposed in the model, since in both scenarios the optimizer adjusts the variables to produce the required quantity, as shown in the following Figure 4.15 and Figure 4.16 for AWE and PEM scenarios, respectively.

In the PEM electrolyzer simulation, the model's sensitivity is clear. From Day 3 to Day 7, as shown in Figure 4.16, the optimizer enforces sharp reductions in power input, significantly decreasing hydrogen production. This occurs because, during these periods, it's more economically advantageous to sell the available renewable energy to the grid rather than use it as feedstock for hydrogen generation. This behaviour becomes even more pronounced in the daily hydrogen production data, where, from Day 5 to Day 7, the model operates at the minimum required output, as illustrated in Figure 4.16. Without this production constraint, both systems would likely produce very little hydrogen or even shut down entirely during times when selling electricity is more profitable.

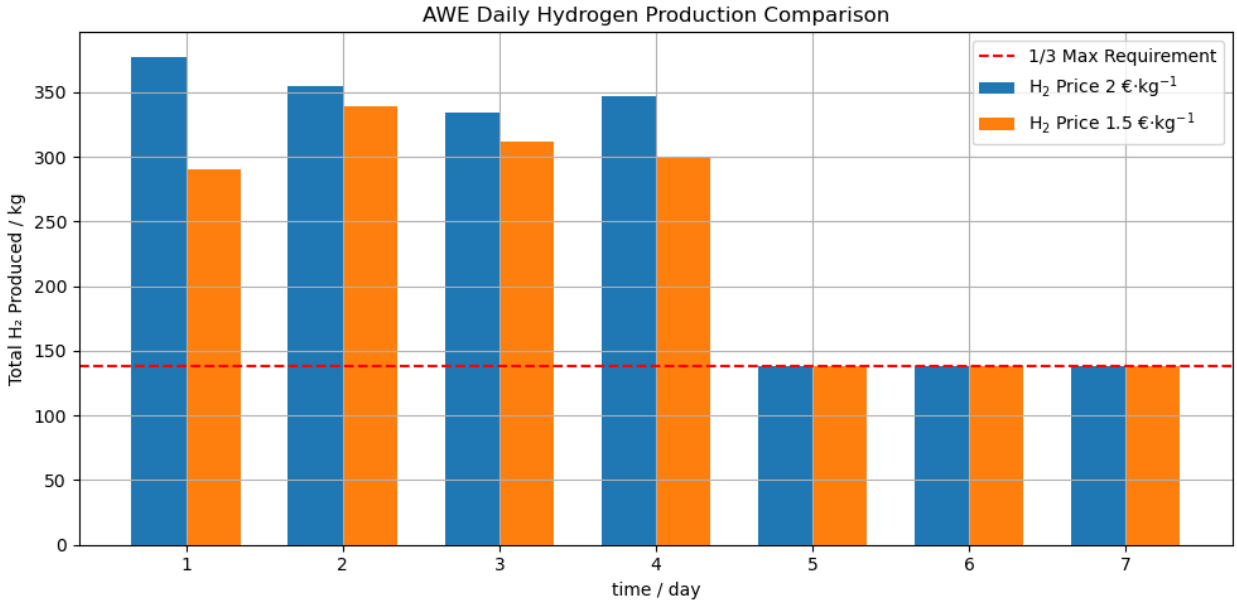

Figure 4.15 - Daily hydrogen production for each simulation day and the respective production constraint with different hydrogen prices and grid price uncertainty obtained by CasADi in the normal week for AWE

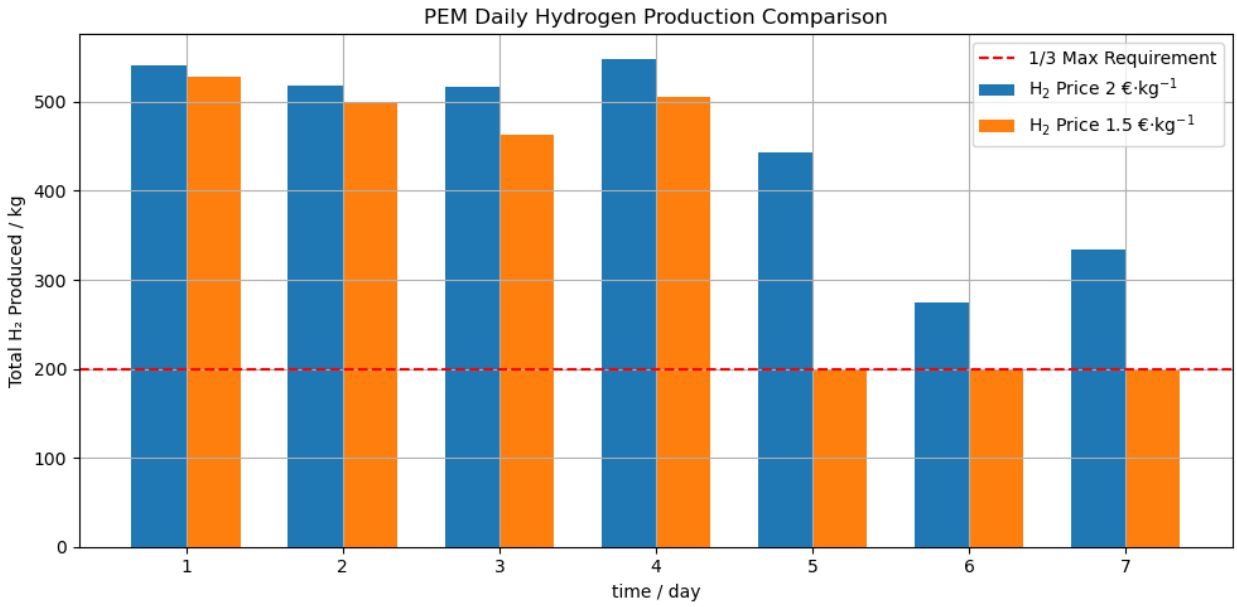

Figure 4.16 - Daily hydrogen production for each simulation day and the respective production constraint with different hydrogen prices and grid price uncertainty obtained by CasADi in the normal week for PEM

5. Conclusion

The current work provides crucial insights into the operational flexibility and economic responsiveness of AWE and PEM electrolyzer systems under varying scenarios.

In the base scenario, the objective is to maximize the profit by optimally managing hydrogen production and energy flows. The system can either utilize available renewable energy to produce hydrogen or sell energy back to the grid. Additionally, it is allowed to purchase electricity from the grid to supplement renewables when economically advantageous. The hydrogen production process is controlled by adjusting current and cooling water, allowing the system to dynamically respond to energy price fluctuations and operational constraints. When hydrogen production is profitable, the optimizer increases current and cooling to maintain optimal temperature and efficiency. When it is not profitable, current and temperature drop, and surplus renewable energy is sold to the grid. Both AWE and PEM models follow this principle but differ in operation: AWE tends to reduce or stop production during high electricity prices to sell power, while PEM continues producing at lower power due to its higher efficiency, sometimes even buying grid power during peak prices to maintain hydrogen output. Outside peak hours, both models buy grid power to operate near nominal levels. Although grid prices mainly guide decisions, the optimizer occasionally prioritizes overall economic benefit, showing a nuanced strategy.

In the electricity price variation and deviation scenario, the study highlights the strategic behaviour of both systems when subject to economic signals from the grid, particularly under a rolling optimization framework. The results demonstrate that electricity price is a key factor influencing system operation. Lower grid prices encourage increased hydrogen production, as it becomes more cost-effective to purchase electricity for the electrolyzer and less cost-effective to sell electricity. Conversely, higher prices incentivize selling excess renewable energy to the grid rather than producing hydrogen. This dual response, buying electricity during low-price periods and selling renewable energy during high-price periods, enhances system flexibility and overall profitability. This behaviour is especially evident in the PEM electrolyzer system, which shows greater sensitivity to price fluctuations. From Day 2 to Day 5, the optimizer often minimizes operating periods to align production with economic efficiency rather than simply operating at nominal capacity. In contrast, while the AWE system also responded to price variations, its behaviour remained more stable, especially from Day 5 to Day 7. This is attributed to the daily hydrogen production constraint imposed on the model, which requires a baseline level of production. The constraint effectively curtails the system’s flexibility, forcing it to operate at higher levels even during periods when selling electricity would be more beneficial. Nevertheless,

the optimizer still leveraged downtime where possible, particularly in the early days of the simulation, reflecting a balance between economic optimization and constraint satisfaction.

The comparative analysis between the two technologies underlines the value of price sensitivity modelling in energy system optimization. Notably, the inclusion of a rolling optimization strategy significantly enhanced the model's capacity to adapt to short-term price changes, showcasing its practical relevance in real-time market operations. The decision to exclude high-price hydrogen scenarios was justified, as they would predictably lead to continuous operation at nominal capacity, offering limited additional insights into system behaviour under economically constrained conditions. The hydrogen price reduction scenario showed that lower prices lead to longer and sharper shutdowns in both AWE and PEM systems, especially early in the period. AWE maintained stable production later due to hydrogen output constraints, while PEM reduced hydrogen output significantly, preferring to sell excess renewable energy to the grid. Without the daily production constraint, both systems would minimize hydrogen production or shut down when selling electricity is more profitable.

Ultimately, this study underscores the importance of incorporating real-time market dynamics, such as electricity price volatility and intermittent renewable energy production, into hydrogen production strategies. It is important to note that this work did not aim to determine which electrolyzer technology is superior. The focus here was on assessing each system’s sensitivity and operational response to real-time economic scenarios and grid conditions. These findings can inform future policy and investment decisions by emphasizing the conditions under which hydrogen systems can be economically competitive, particularly when dynamic grid participation is considered. Future research should further explore multi-scenario simulations including storage dynamics, demand-side interactions, and the effects of more granular price forecasting on system optimization.

6. Assessment of the work done

6.1. Objectives Achieved

This work aimed to evaluate the operational performance of AWE and PEM electrolyzers under dynamic electricity market conditions using optimal control strategies. All objectives were successfully addressed through model-based simulations and real-time case studies.

Both electrolyzer systems were implemented in a unified optimization framework, developed using Python and CasADi, demonstrating their dynamic behaviour and responsiveness to fluctuating electricity prices and renewable energy production.

The proposed approach allowed for a flexible and economical comparison of the system performance, offering insights into their practical integration into renewable-based energy systems.

6.2. Contribution to the Sustainable Development Goals

Table 6.1- Contribution to the Sustainable Development Goals [31]

SDG	Goal	Contribution	Performance indicators and metrics
7	2	This work directly supports the increased integration of variable renewable electricity sources into energy systems by optimizing the operational flexibility of electrolyzers. It demonstrates how hydrogen production can absorb electricity surpluses, enhancing grid stability and enabling a higher penetration of renewable energies.	Achieved enhanced flexibility in absorbing renewable energy surpluses in simulations. Showcased the ability of optimal control strategies to balance electrolyzer operation with intermittent renewable power availability.
	3	By applying optimal control strategies, the research improves the overall energy efficiency of the green hydrogen production process. This minimizes energy waste during electrolysis, contributing to more efficient utilization of renewable power.	Optimal control strategies demonstrated significant improvements in operational economics and energy efficiency for hydrogen production compared to rule-based approaches.

Table 6.1 (continued)

9	4	The dissertation contributes to upgrading energy infrastructure by providing a framework for the intelligent integration of electrolyzers into renewable-rich grids. It promotes the adoption of clean and environmentally sound technologies (green hydrogen production) for industrial processes, enhancing their sustainability.	Development of a unified optimization framework using Python and CasADi for dynamic optimization of electrolyzer systems. Demonstrated improved system responsiveness and suitability for integration into existing and future grid infrastructure.
	5	The development and application of dynamic optimization frameworks (implemented with Python and CasADi) represent significant scientific and technological innovation. This research enhances the technological capabilities for managing and operating advanced electrochemical processes in industrial settings.	The novel application of dynamic optimization using advanced computational techniques (Python, CasADi) represents a direct enhancement of technological capability.
12	2	This research promotes the efficient use of renewable power and water, critical natural resources, for green hydrogen production. By optimizing the electrolysis process, it ensures that these resources are utilized as effectively as possible to meet hydrogen demand.	Optimal control strategies demonstrated efficient utilization of fluctuating renewable power inputs. The qualitative assessment of energy waste reduction contributes to sustainable resource management.
	4	The promotion of green hydrogen production minimizes the generation of greenhouse gas emissions associated with traditional hydrogen production methods, thereby contributing to environmentally sound industrial processes.	The core aim of enabling emissions-free hydrogen production supports a cleaner overall industrial life cycle for hydrogen.

Table 6.1 (continued)

13	2	By enhancing the efficiency and economic viability of green hydrogen production, this work provides crucial insights and a practical framework that can inform national strategies and policies aimed at decarbonization. It demonstrates a pathway for integrating emissions-free hydrogen into the broader energy system.	The qualitative assessment of each technology's adaptability and cost-effectiveness under real-world market conditions provides data relevant for strategic planning of hydrogen economies.
	3	As a scientific dissertation, this work directly contributes to the body of knowledge surrounding climate change mitigation technologies (in particular, green hydrogen). It enhances understanding and capacity within the scientific and engineering communities regarding optimal operation of decarbonization assets.	The research findings and methodology provide a basis for further academic discourse and inform future research and development in climate change mitigation technologies.

6.3. Final Assessment

This dissertation delivers a very important and interesting contribution, effectively demonstrating the dynamic optimization of AWE and PEM electrolyzer systems. Not only does it provide a robust framework for understanding their operational behavior under fluctuating market conditions, but it also serves as a crucial foundation for adapting these techniques to other dynamic energy systems or for developing even more sophisticated models for green hydrogen production. The methodologies and findings presented here, particularly the unified optimization framework developed with Python and CasADi, offer valuable insights and a solid framework for further research and practical applications. This makes the dissertation a significant and engaging contribution to the field of sustainable energy systems and real-time energy management.

7. References

[1] Dincer, I., AlZahrani, A.A. *Electrolyzers*. *Comprehensive Energy Systems*, 4, 985–1025 (2018). https://doi.org/10.1016/B978-0-12-809597-3.00442-9

[2] Wei, X., Sharma, S., Waeber, A., Wen, D., Sampathkumar, S.N., Margni, M., Maréchal, F., Van Herle, J. Comparative life cycle analysis of electrolyzer technologies for hydrogen production: Manufacturing and operations. *Joule*, 8, 3347-3372 (2024). https://doi.org/10.1016/j.joule.2024.09.007

[3] Xu, H., Ni, M. High-temperature electrolysis and co-electrolysis. *Power to Fuel: How to Speed Up a Hydrogen Economy*, 51–73 (2021)

[4] Sebbahi, S., Assila, A., Belghiti, A.A., Laasri, S., Kaya, S., Hlil, E.K., Rachidi, S., Hajjaji, A. A comprehensive review of recent advances in alkaline water electrolysis for hydrogen production. *International Journal of Hydrogen Energy*, 82, 583-599 (2024) https://doi.org/10.1016/j.ijhydene.2024.07.428

[5] Martinez Lopez, V.A., Ziar, H., Haverkort, J.W., Zeman, M., Isabella, O. Dynamic operation of water electrolyzers: A review for applications in photovoltaic systems integration. *Renewable and Sustainable Energy Reviews*, 182, 113407 (2023). https://doi.org/10.1016/j.rser.2023.113407

[6] Bakker, M.M., Vermaas, D.A. Gas bubble removal in alkaline water electrolysis with utilization of pressure swings. *Electrochimica Acta*, 319, 148–157 (2019). https://doi.org/10.1016/j.electacta.2019.06.049

[7] Carmo, M., Fritz, D.L., Mergel, J., Stolten, D. A comprehensive review on PEM water electrolysis. *International Journal of Hydrogen Energy*, 38(12), 4901–4934 (2013). https://doi.org/10.1016/j.ijhydene.2013.01.151

[8] Zeng, K., Zhang, D. Recent progress in alkaline water electrolysis for hydrogen production and applications. *Progress in Energy and Combustion Science*, 36(3), 307–326 (2010). https://doi.org/10.1016/j.pecs.2009.11.002

[9] Brauns, J., Turek, T. Model-Based Analysis and Optimization of Pressurized Alkaline Water Electrolysis Powered by Renewable Energy. *Journal of The Electrochemical Society*, 170(6), 064510 (2023). https://doi.org/10.1149/1945-7111/acd9f1

[10] Hammoudi, M., Henao, C., Agbossou, K., Dubé, Y., Doumbia, M.L. New multi-physics approach for modelling and design of alkaline electrolyzers. *International Journal of Hydrogen Energy*, 37(19), 13895–13913 (2012). https://doi.org/10.1016/j.ijhydene.2012.07.015

[11] Candelino, N.W., Jalili, N. *Dynamic Systems and Control Engineering*. Cambridge University Press, Cambridge (2023).

[12] Andersson, J., Birn, J., Johansson, K.H. CasADi: A Software Framework for Nonlinear Optimization and Optimal Control. *20th International Symposium on Mathematical Programming* (2019).

[13] *"CasADi"*. *CasADi*. Acessed March 11, 2025. https://web.casadi.org/

[14] Tao, M., Azzolini, J.A., Stechel, E.B., Ayers, K.E., Valdez, T.I. Review—Engineering Challenges in Green Hydrogen Production Systems. *Journal of The Electrochemical Society*, 169(5), 054503 (2022). https://doi.org/10.1149/1945-7111/ac6983

[15] Bollmann, J., Pitchaimuthu, S., Kühnel, M.F. Challenges of Industrial-Scale Testing Infrastructure for Green Hydrogen Technologies. *Energies*, 16(8), 3604 (2023). https://doi.org/10.3390/en16083604

[16] NEL Hydrogen. *A485 Series Alkaline Electrolyser Stack and Electrolyte System Module – Technical Data Sheet*. Accessed March 28, 2025. Retrieved from https://nelhydrogen.com/resources/a485-series-alkaline-electrolyser-stack-and-electrolyte-system-module/

[17] Hamdan, M., Harrison, K. *MW-Scale PEM-Based Electrolyzers for RES Applications*. DOE Hydrogen and Fuel Cells Program 2019 Annual Merit Review and Peer Evaluation Meeting, Poster Session. Giner ELX & National Renewable Energy Laboratory (2019). https://www.hydrogen.energy.gov/pdfs/review19/h2007_harrison_2019_p.pdf

[18] MSE Supplies LLC. MSE PRO MA-L-0.5A PEM Water Electrolyzer Stack, Max. Flow Rate 0.5 Nm^3/h – Technical Data Sheet. Accessed March 28, 2025. Retrieved from https://www.msesupplies.com/products/mse-pro-ma-l-0-5a-pem-water-electrolyzer-stack-max-flow-rate-0-5-nm3-h

[19] Jiang, Y.-C., Dong, S.-M., Liang, Z., Wang, X.-L., Shi, L., Yan, B., Zhao, T. Holistic Dynamic Modeling and Simulation of Alkaline Water Electrolysis Systems Based on Heat Current Method. *Energies*, 17(23), 6202 (2024). https://doi.org/10.3390/en17236202

[20] Abdin, Z., Webb, C.J., Gray, E.MacA. Modelling and simulation of an alkaline electrolyser cell. Energy, 138, 316–331 (2017). https://doi.org/10.1016/j.energy.2017.07.053

[21] Deng, X., Yang, F., Li, Y., Dang, J., Ouyang, M. *Quantitative study on gas evolution effects under large current density in zero-gap alkaline water electrolyzers*. *Journal of Power Sources*, 555, 232378 (2023). https://doi.org/10.1016/j.jpowsour.2022.232378

[22] Asiaban, S., Bozalakov, D., Vandevelde, L. *Development of a dynamic mathematical model of PEM electrolyser for integration into large-scale power systems*. *Energy Conversion and Management: X*, 23, 100610 (2024). https://doi.org/10.1016/j.ecmx.2024.100610

[23] Koundi, M., El Fadil, H., EL Idrissi, Z., Lassioui, A., Intidam, A., Bouanou, T., Nady, S., Rachid, A. Investigation of Hydrogen Production System-Based PEM EL: PEM EL Modeling, DC/DC Power Converter, and Controller Design Approaches. *Clean Technologies*, 5(2), 531–568 (2023). https://doi.org/10.3390/cleantechnol5020028

[24] Qi, R., Li, J., Lin, J., Song, Y., Wang, J., Cui, Q., Qiu, Y., Tang, M., & Wang, J. Thermal modeling and controller design of an alkaline electrolysis system under dynamic operating conditions. *Applied Energy*, 332, 120551 (2023). https://doi.org/10.1016/j.apenergy.2022.120551

[25] Luo, K., Li, P., Yan, Y., Ding, C., Liu, Z., Huang, S., Duan, Z., & Cai, L. Dynamic performance prediction of PEM electrolyzers combining an electrochemical neural network model and a lumped thermal capacitance model. *International Journal of Green Energy*, January 2025. https://doi.org/10.1080/15435075.2025.2456069

[26] "REN Data Hub." *REN*. Accessed April 26 and May 30, 2025. https://datahub.ren.pt/

[27] Hallemans, N., Howey, D., Battistel, A., Saniee, N.F., Scarpioni, F., Wouters, B., La Mantia, F., Hubin, A., Widanage, W.D., Lataire, J. *Electrochemical impedance spectroscopy beyond linearity and stationarity—A critical review*. *Electrochimica Acta*, 466, 142939 (2023). https://doi.org/10.1016/j.electacta.2023.142939

[28] Lou, F., Chen, D. *Aligned carbon nanostructures based 3D electrodes for energy storage*. *Journal of Energy Chemistry*, 24(5), 559–586 (2015). https://doi.org/10.1016/j.jechem.2015.08.013

[29] Yang, Y., De La Torre, B., Stewart, K., Lair, L., Phan, N.L., Das, R., Gonzalez, D., Lo, R.C. *The scheduling of alkaline water electrolysis for hydrogen production using hybrid energy sources*. *Energy Conversion and Management*, 257, 115408 (2022). https://doi.org/10.1016/j.enconman.2022.115408

[30] Varela, C., Mostafa, M., Zondervan, E. *Modeling alkaline water electrolysis for power-to-x applications: A scheduling approach*. *International Journal of Hydrogen Energy*, 46(14), 9303–9313 (2021). https://doi.org/10.1016/j.ijhydene.2020.12.111

[31] United Nations. *Sustainable Development Goals*. Accessed June 6, 2025. Retrieved from https://sdgs.un.org/goals

Annex A – Additional Simulation Results

This annex presents supplementary graphs from the simulation study that provide further insights into the operational behaviour and performance of the electrolyzer systems under various scenarios. These visualizations support the main analysis by illustrating additional trends, variability, and system responses that were not included in the main body of the thesis but are relevant for a more comprehensive understanding of the results.

Figures A.1 to A.6 and Figures A.7 to A.12 correspond to supplementary data for the base scenario, including cooling water flow, temperature, stack voltage, grid power and price histories, as well as hourly and daily hydrogen production profiles for the AWE and PEM systems, respectively. These graphs offer a more detailed view of the system's day-to-day operation and support the understanding of performance under standard conditions. Figure A.13 represents the renewable power and grid price histories for the base scenario.

Figures A.14 to A.15 (AWE system) and A.16 to A.17 (PEM system) show the electrolyzer power consumption and daily hydrogen production for the normal week under electricity price variations. Similarly, Figures A.19 to A.20 (AWE system) and A.21 to A.22 (PEM system) present the corresponding results for the expensive week. Together, these graphs illustrate how both systems adapt their operation in response to fluctuating electricity prices across different market conditions, with an associated uncertainty value in the electricity prices. Figures A.18 and A.23 represent the renewable power and grid price histories for the normal and expensive week, respectively.

Figures A.24 and A.25 show the electrolyzer power consumption and grid price histories for the AWE and PEM systems, respectively, during the normal week with hydrogen price reduction and grid price uncertainty. These graphs illustrate how the systems adjust their operation in response to changing hydrogen market conditions.

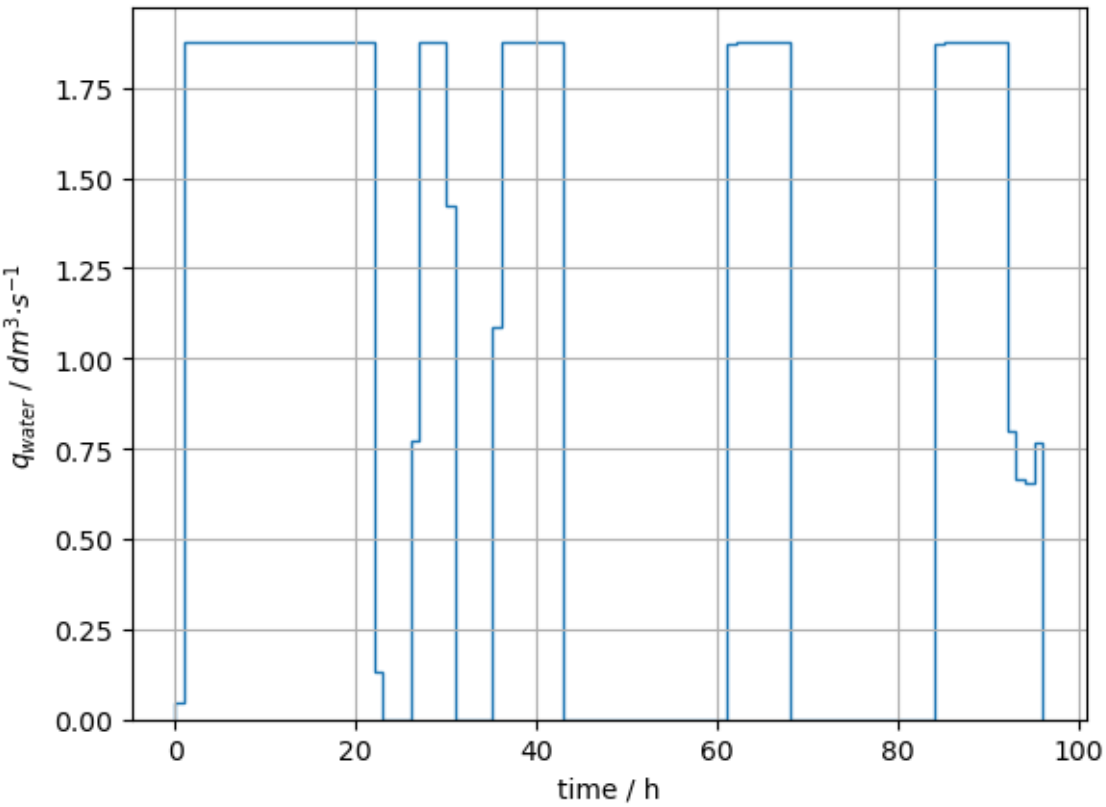

Figure A.1 – Cooling water trajectory obtained by CasADi for the AWE model

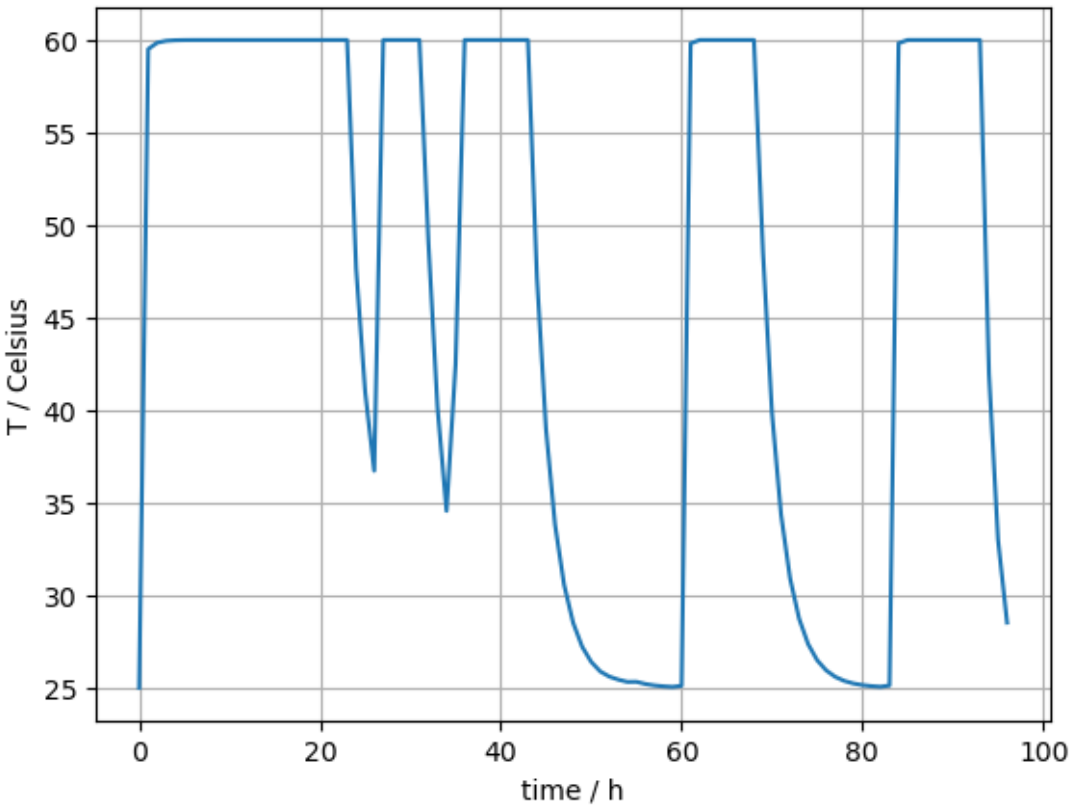

Figure A.2 – Temperature trajectory obtained by CasADi for the AWE model

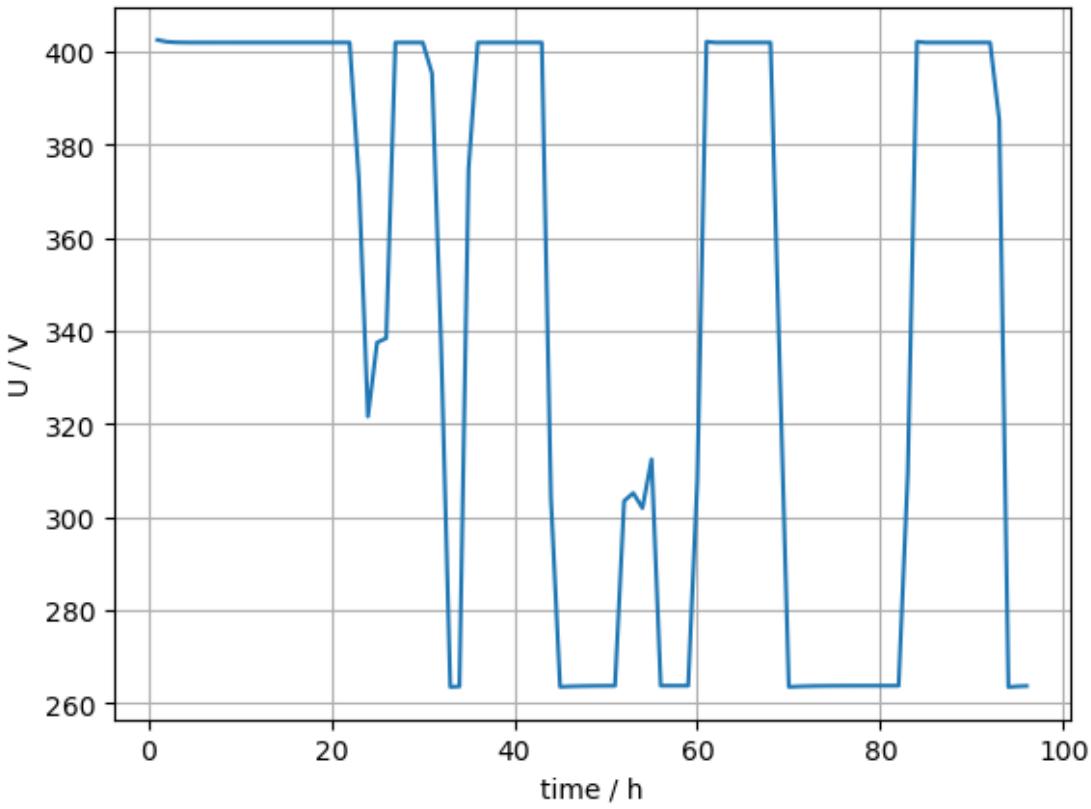

Figure A.3 – Stack voltage trajectory obtained by CasADi for the AWE model in the base scenario

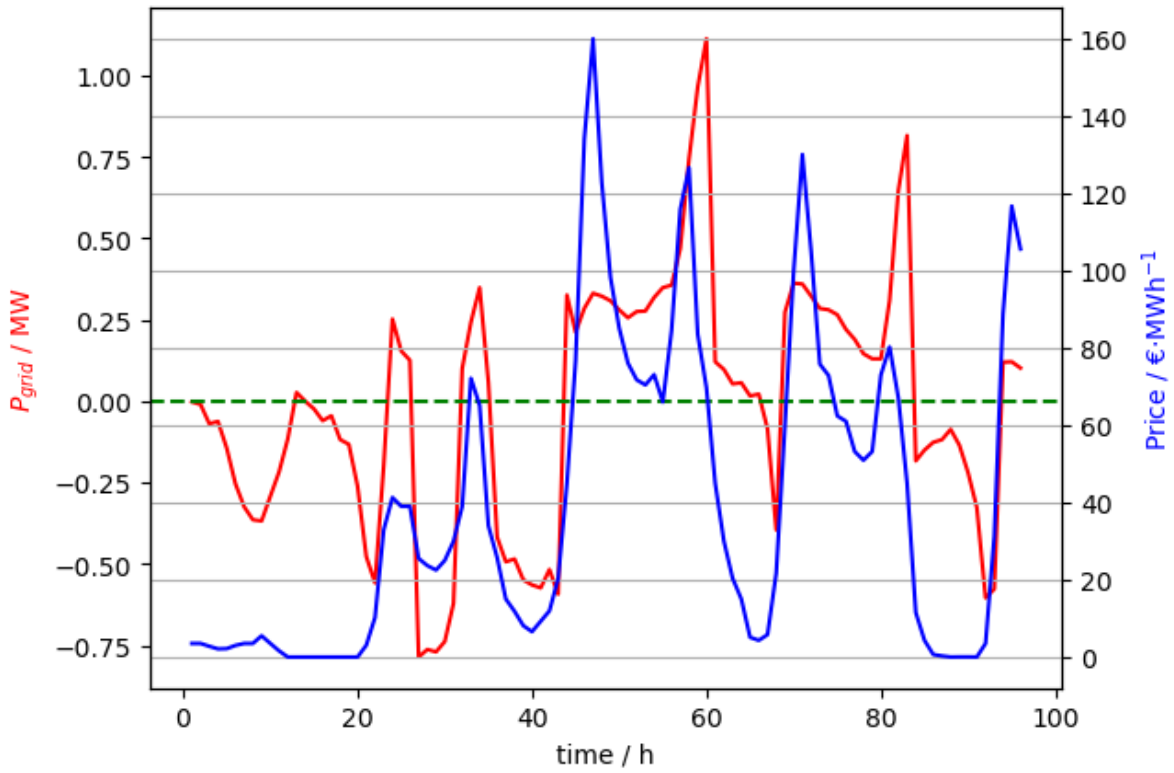

Figure A.4 - Grid power and price histories obtained by CasADi for the AWE model in the base scenario

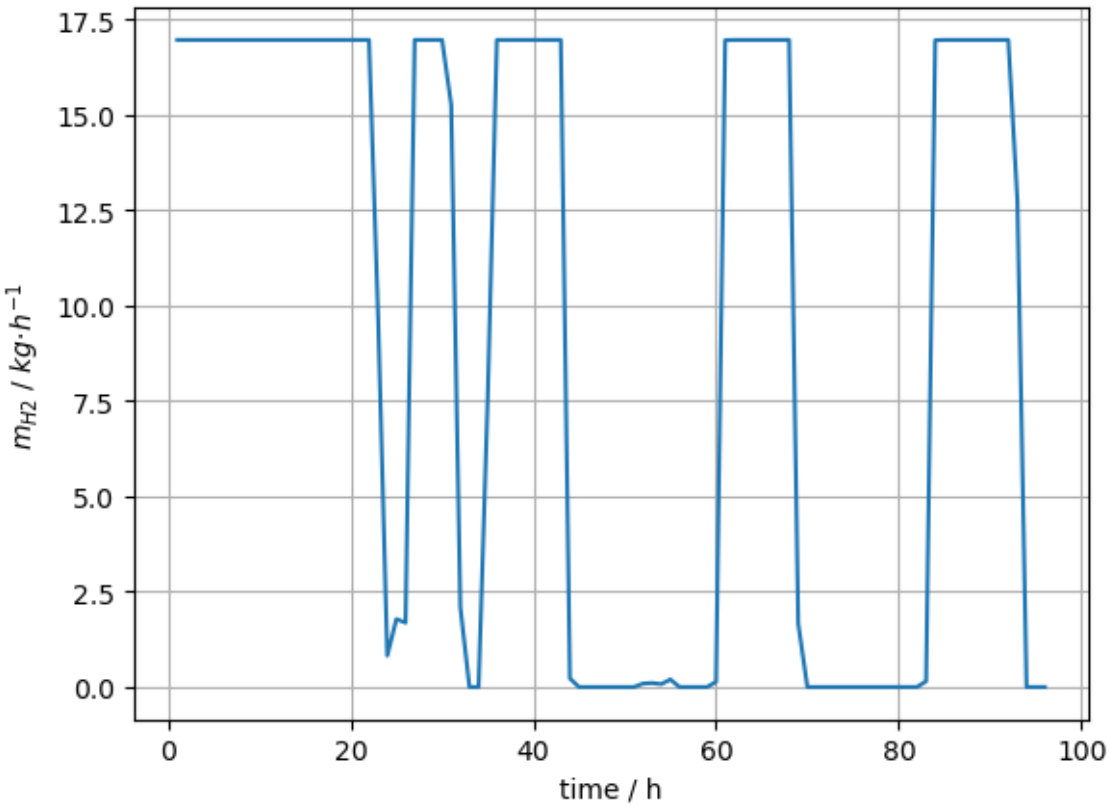

Figure A.5 – Hydrogen production history obtained by CasADi for the AWE model in the base scenario

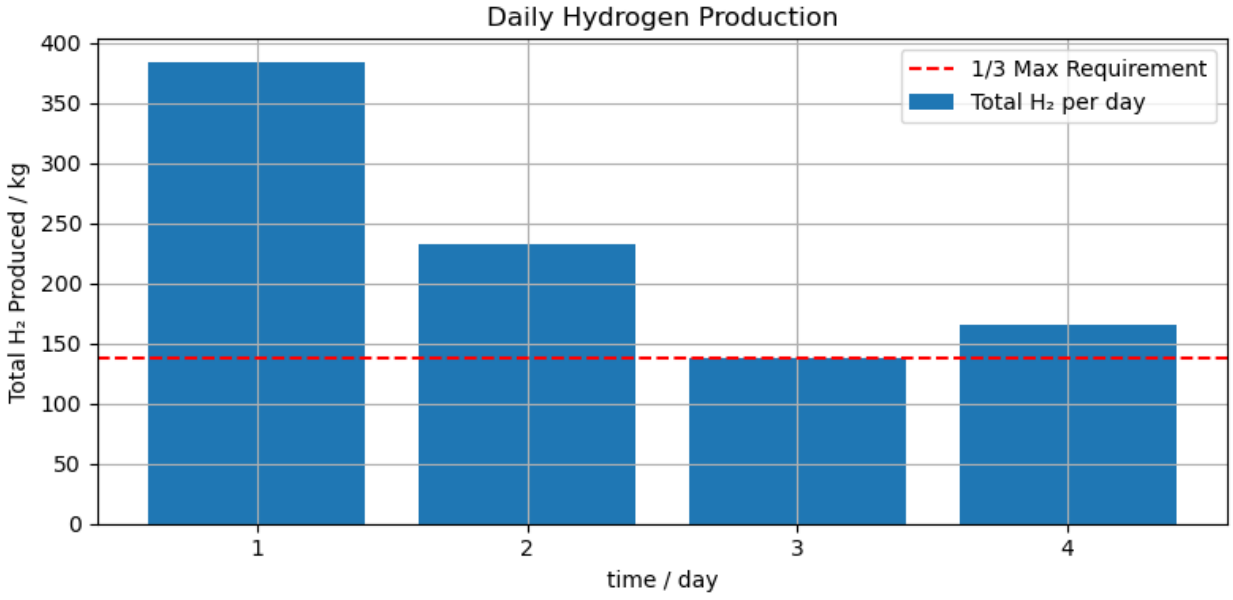

Figure A.6 – Daily hydrogen production for each simulation day and the respective production constraint obtained by CasADi for the AWE model in the base scenario

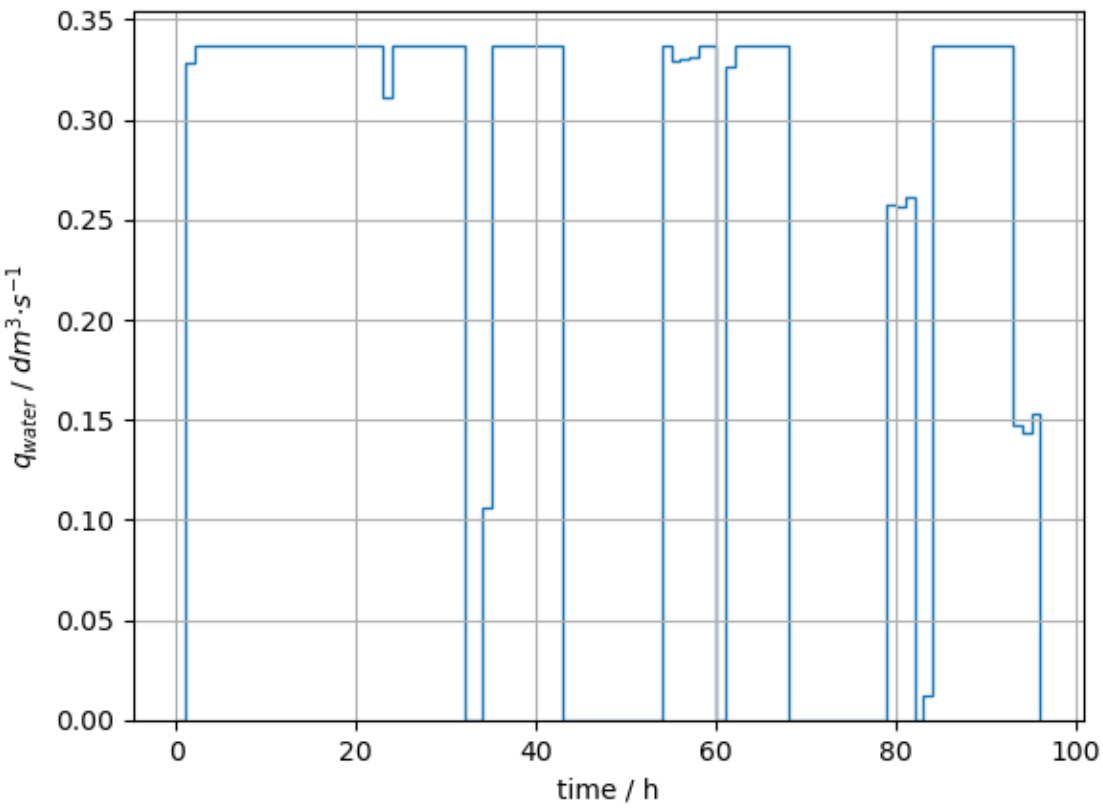

Figure A.7 – Cooling water trajectory obtained by CasADi for the PEM model

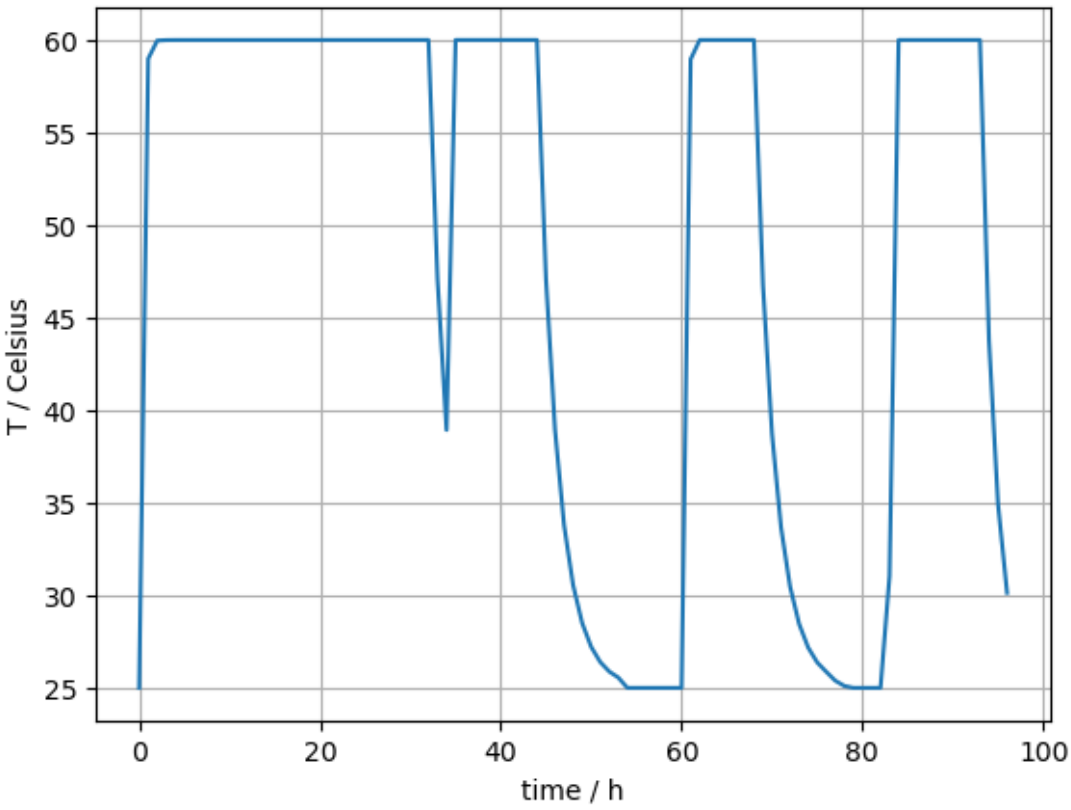

Figure A.8 - Temperature trajectory obtained by CasADi for the PEM model

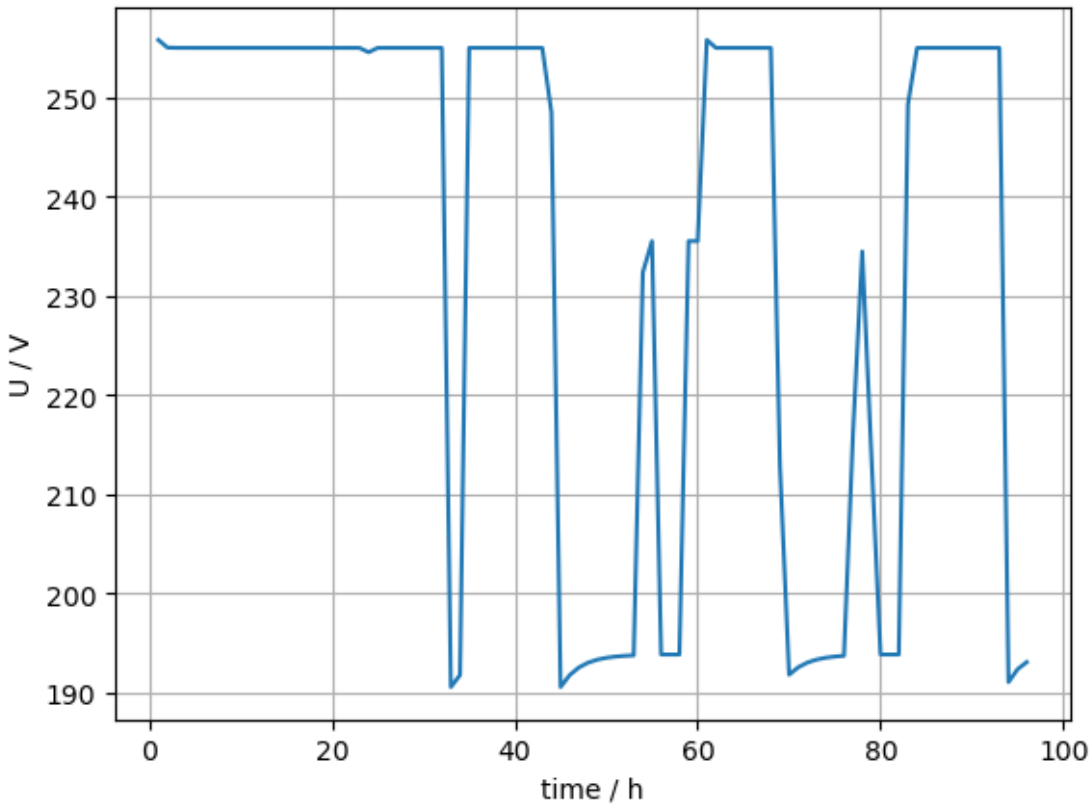

Figure A.9 – Stack voltage trajectory obtained by CasADi for the PEM model in the base scenario

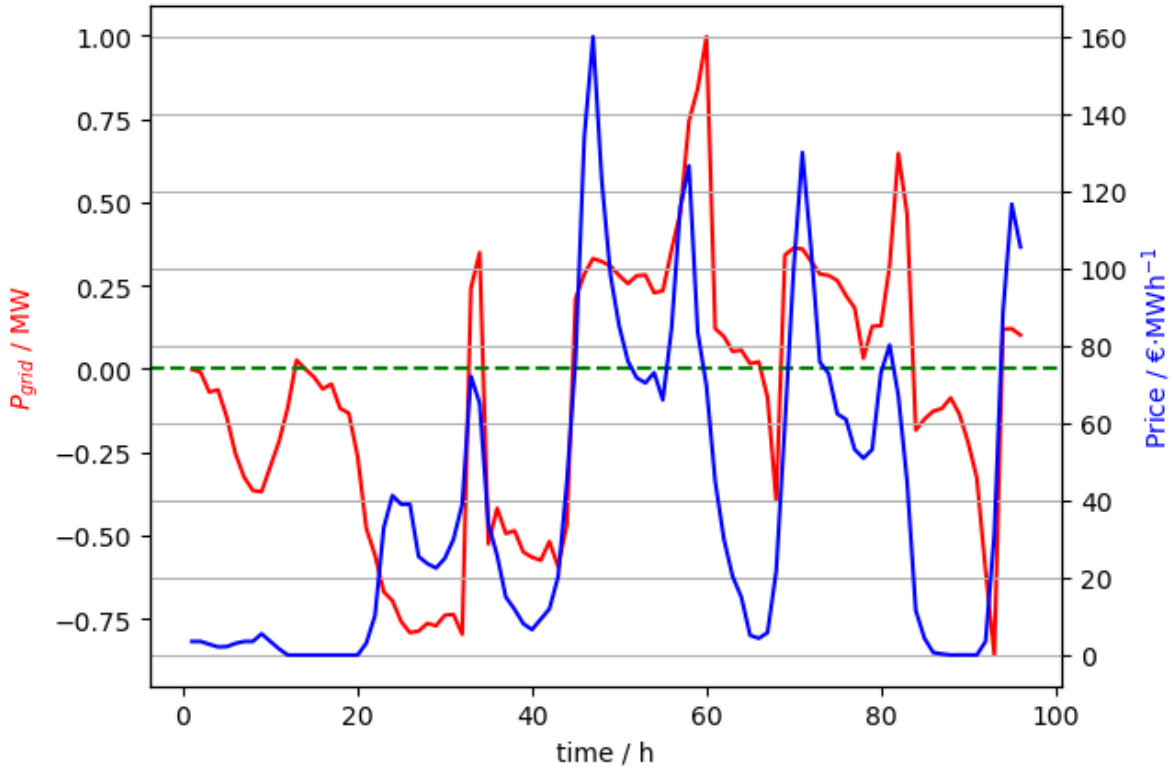

Figure A.10 - Grid power and price histories obtained by CasADi for the PEM model in the base scenario

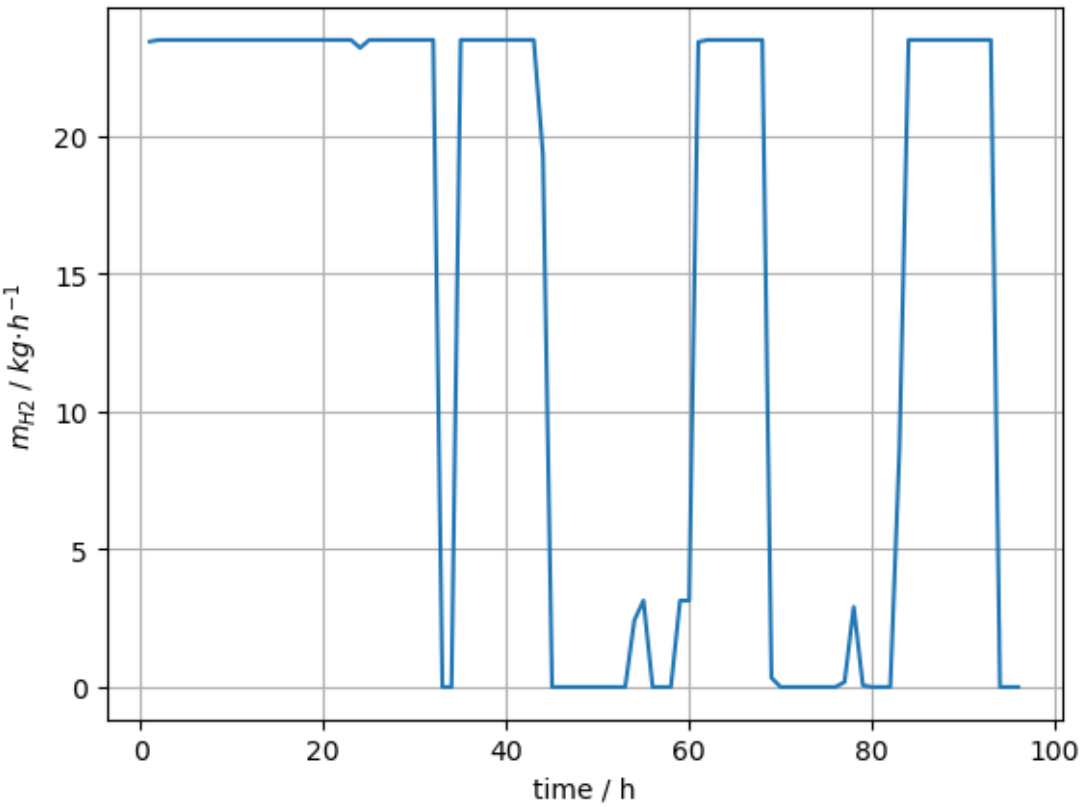

Figure A.11 - Hydrogen production history obtained by CasADi for the PEM model in the base scenario

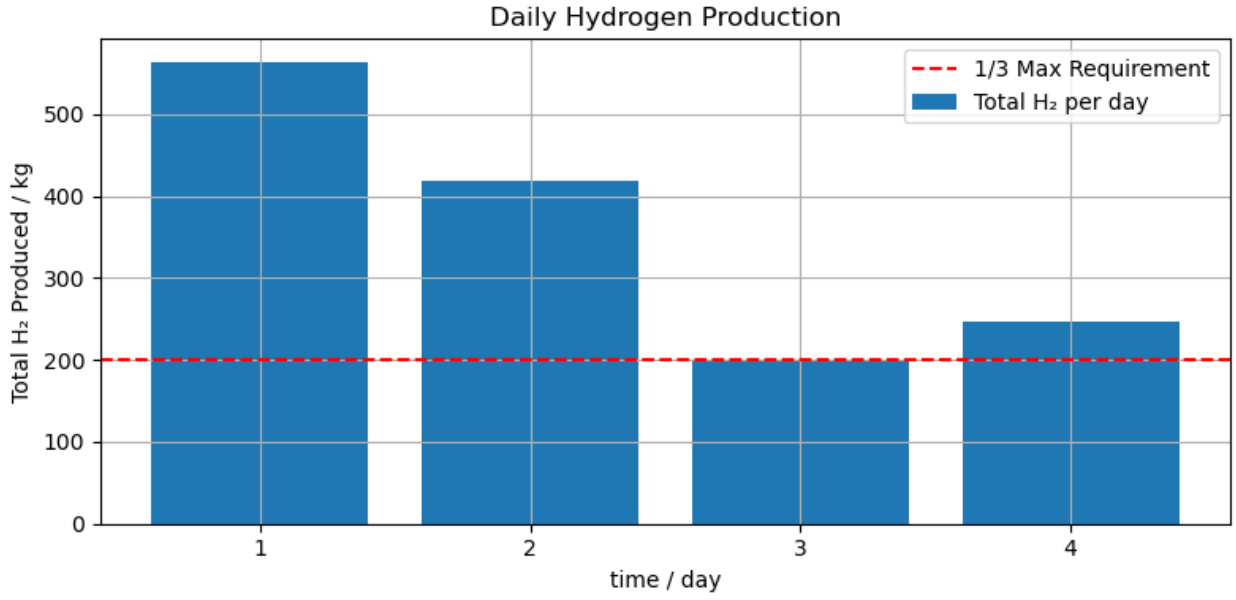

Figure A.12 - Daily hydrogen production for each simulation day and the respective production constraint obtained by CasADi for the PEM model in the base scenario

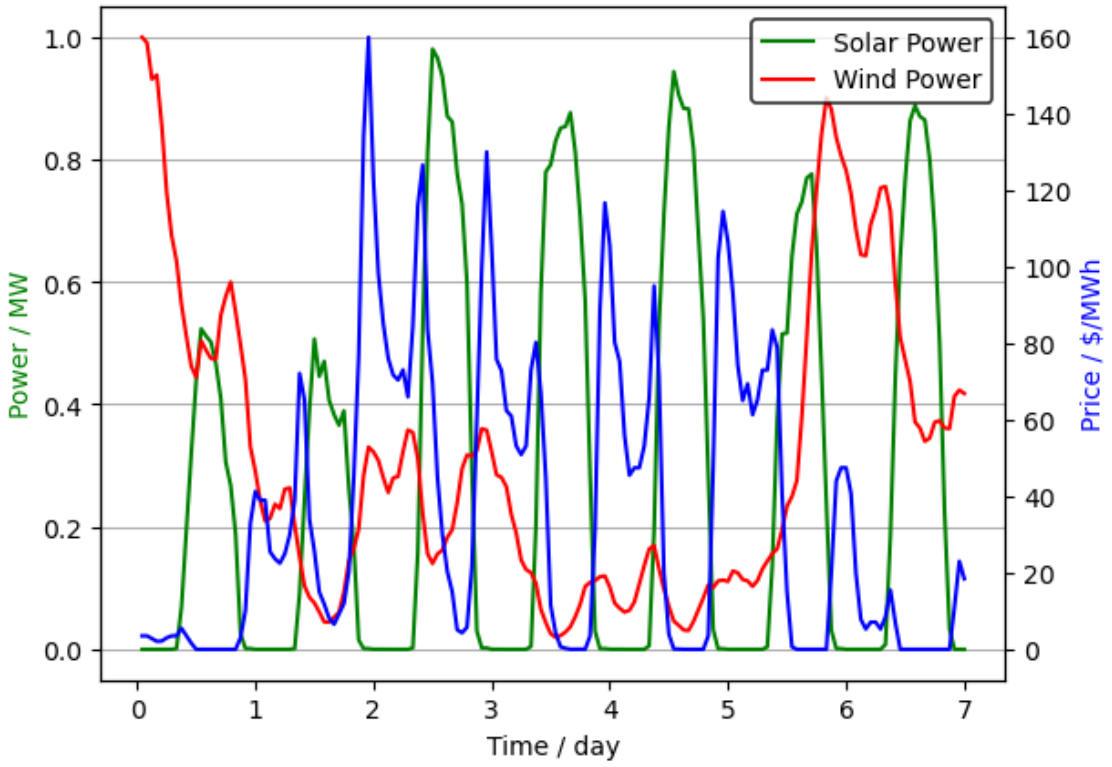

Figure A.13 – Renewable power and grid price histories for both models in the base scenario

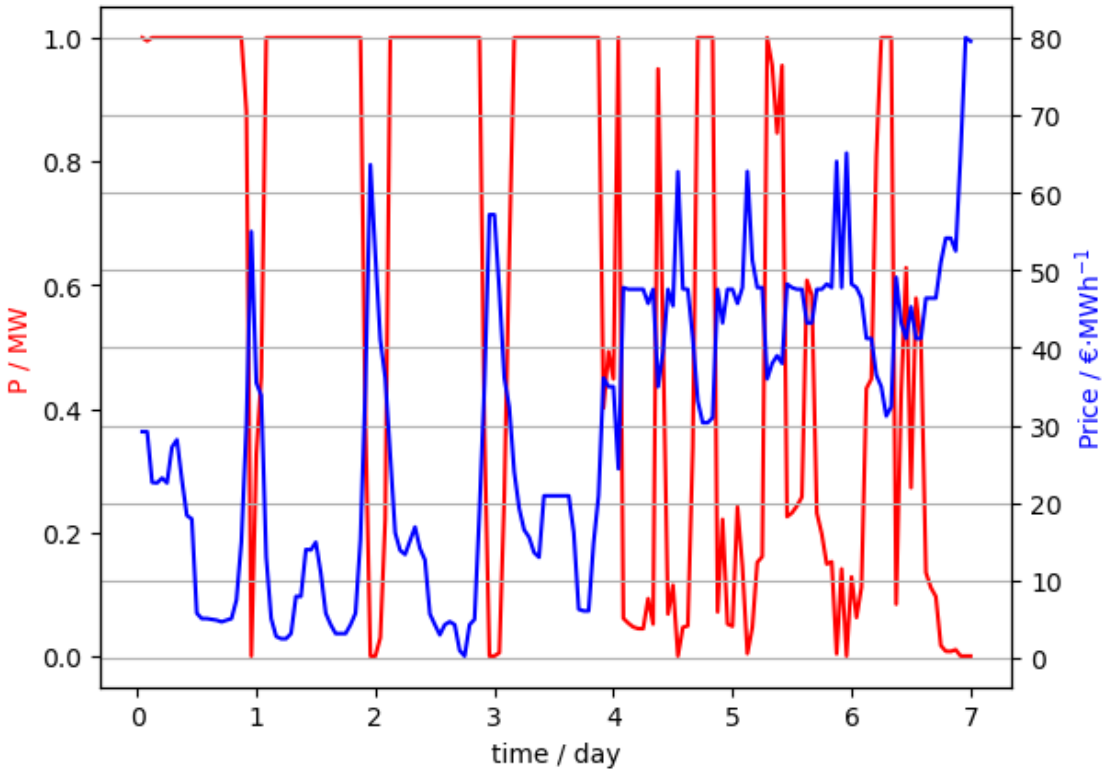

Figure A.14 – Electrolyzer power consumption and grid prices histories obtained by CasADi for the AWE model in the normal week in the grid price variation scenario

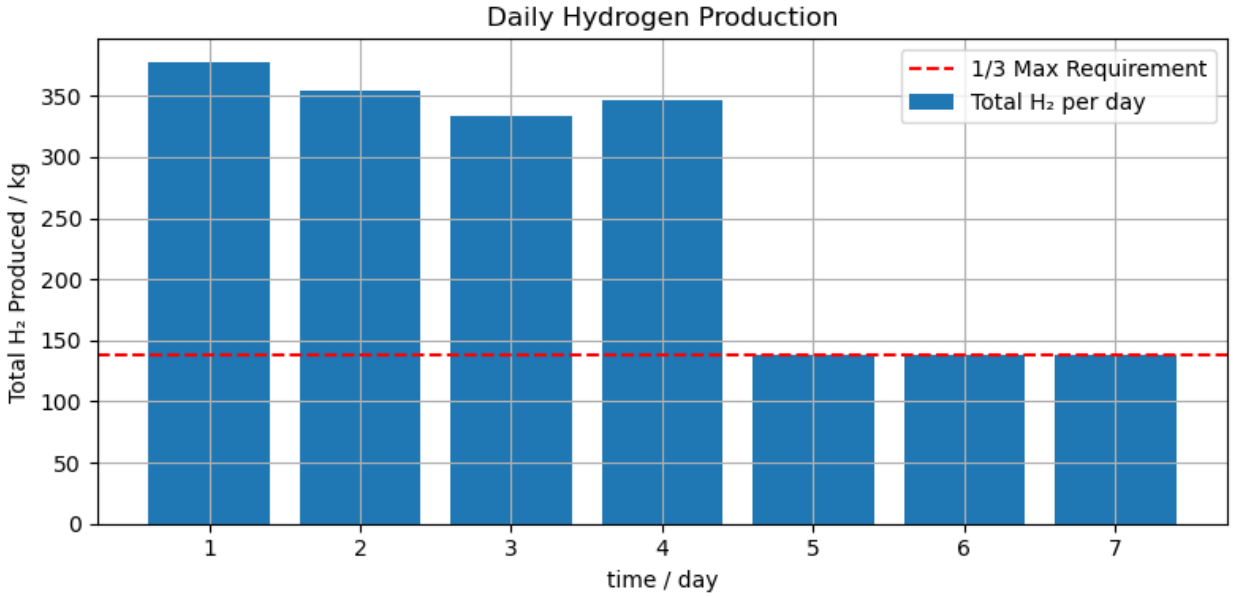

Figure A.15- Daily hydrogen production for each simulation day and the respective production constraint in the normal week obtained by CasADi for the AWE model in the grid price variation scenario

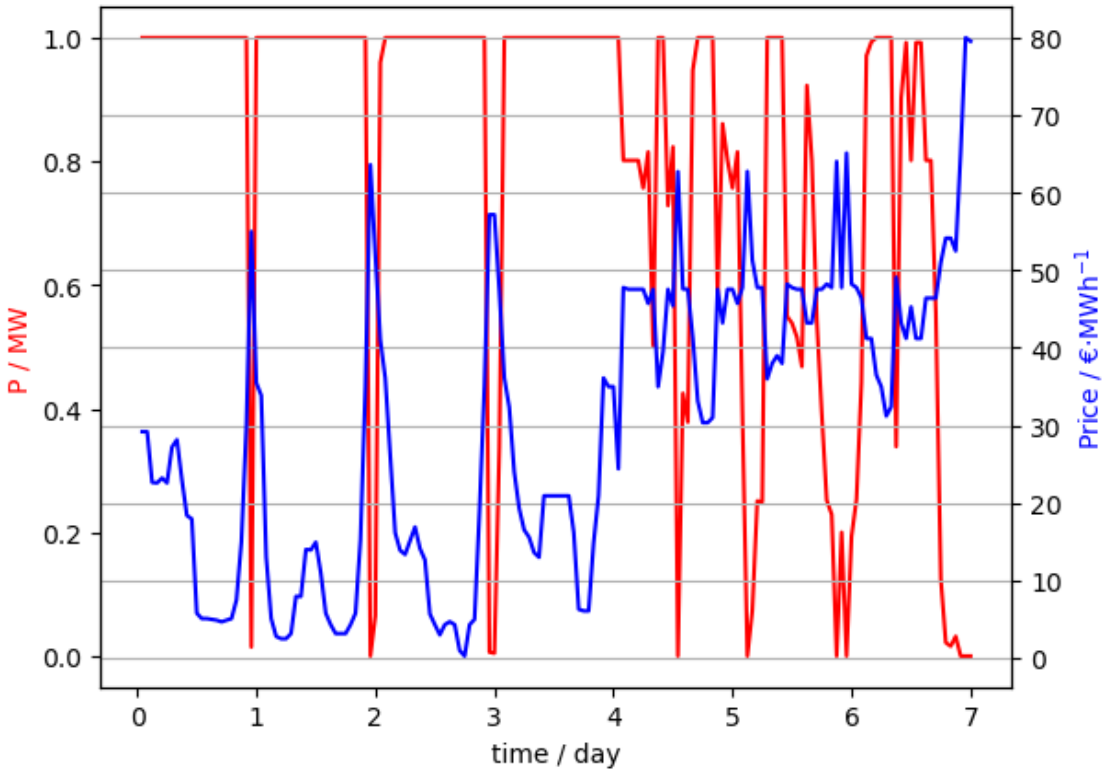

Figure A.16 – Electrolyzer power consumption and grid prices histories obtained by CasADi for the PEM model in the normal week in the grid price variation scenario

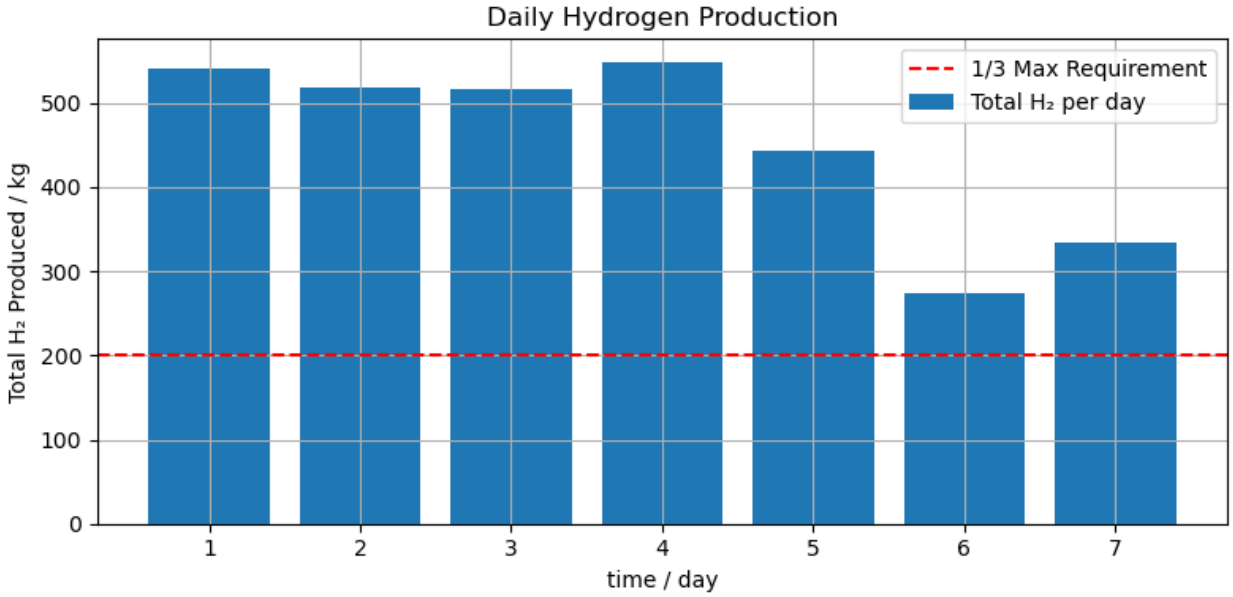

Figure A.17 - Daily hydrogen production for each simulation day and the respective production constraint in the normal week obtained by CasADi for the PEM model in the grid price variation scenario

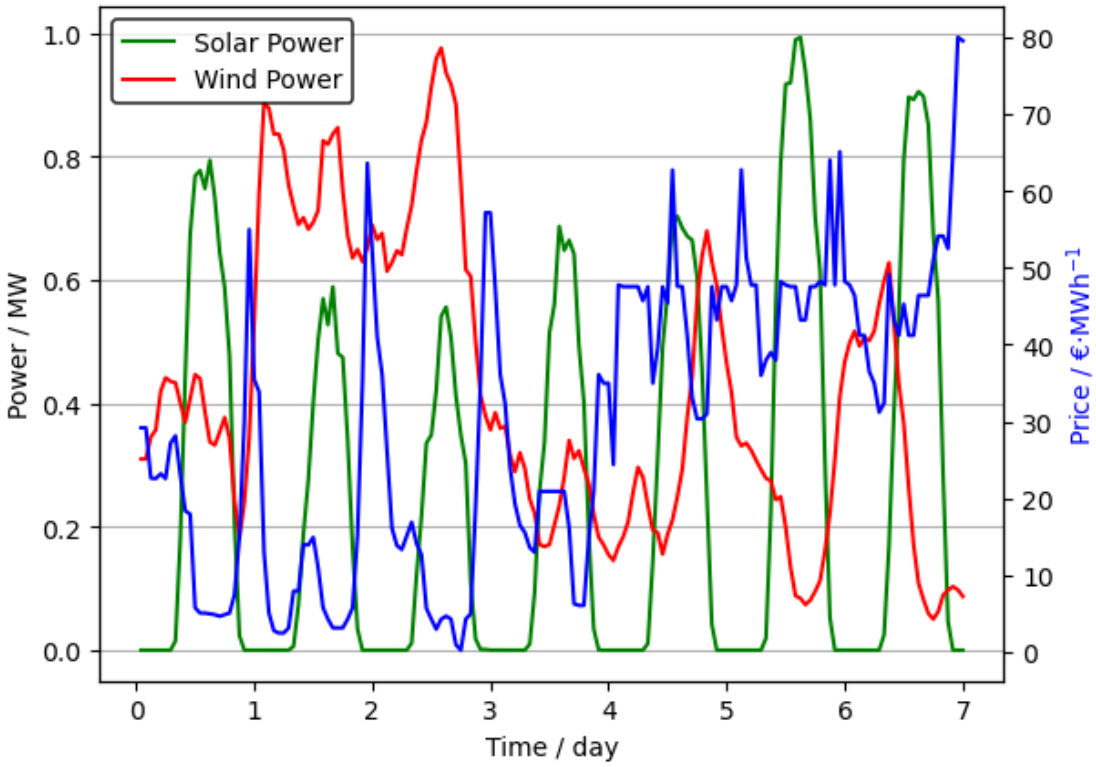

Figure A.18 - Renewable power and grid price histories in the normal week obtained by CasADi for both models in the grid price variation scenario

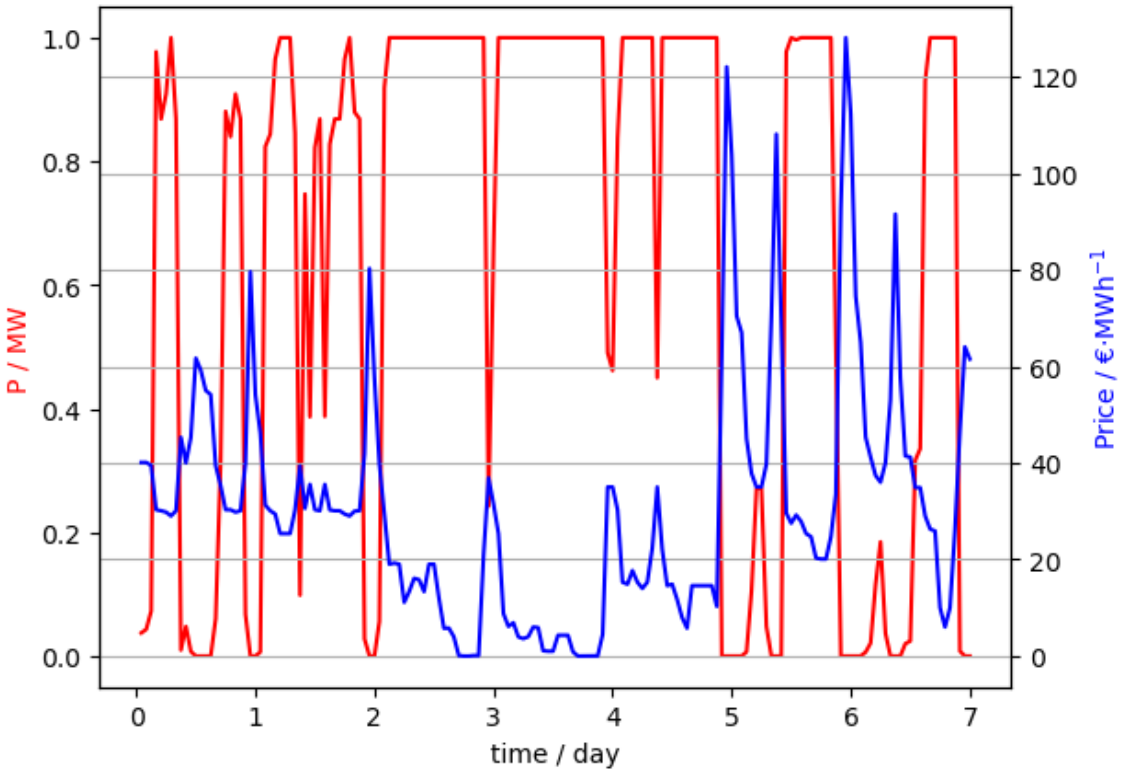

Figure A.19 - Electrolyzer power consumption and grid prices histories obtained by CasADi for the AWE model in the expensive week in the grid price variation scenario

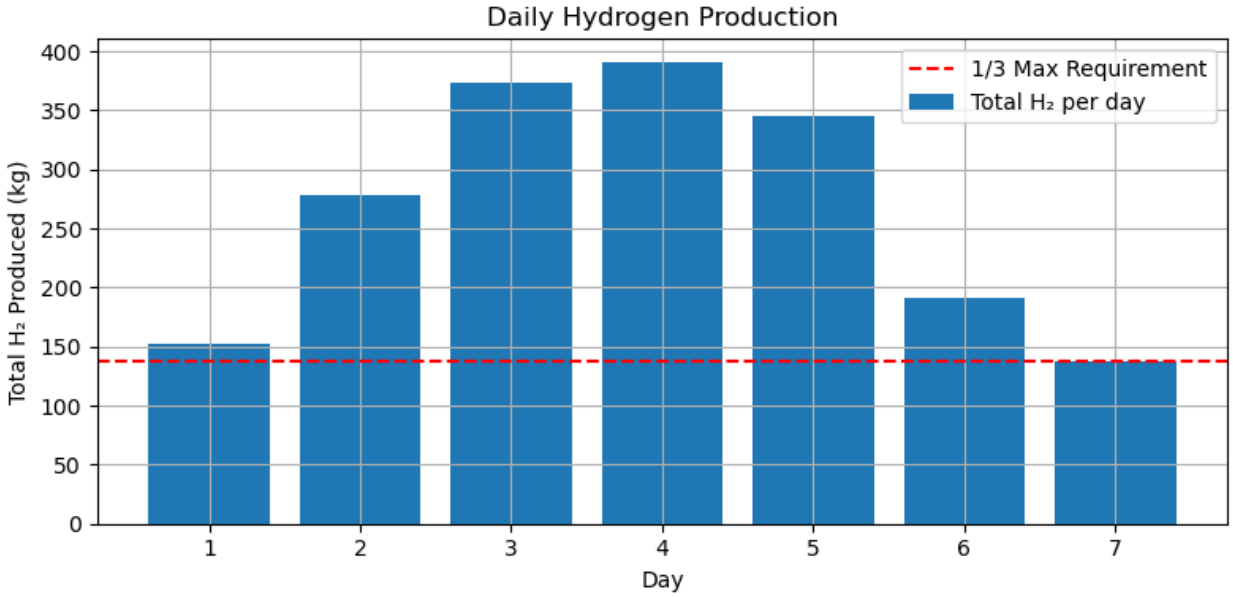

Figure A.20 - Daily hydrogen production for each simulation day and the respective production constraint in the expensive week obtained by CasADi for the AWE model in the grid price variation scenario

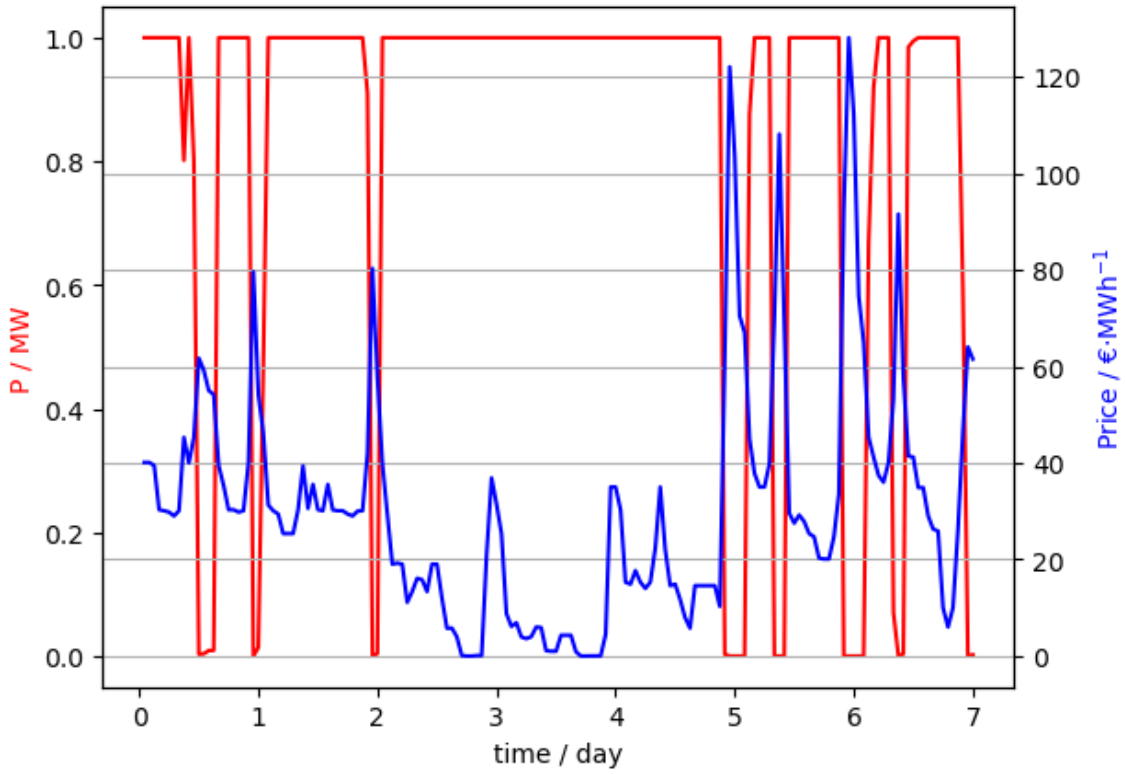

Figure A.21 - Electrolyzer power consumption and grid prices histories obtained by CasADi for the PEM model in the expensive week in the grid price variation scenario

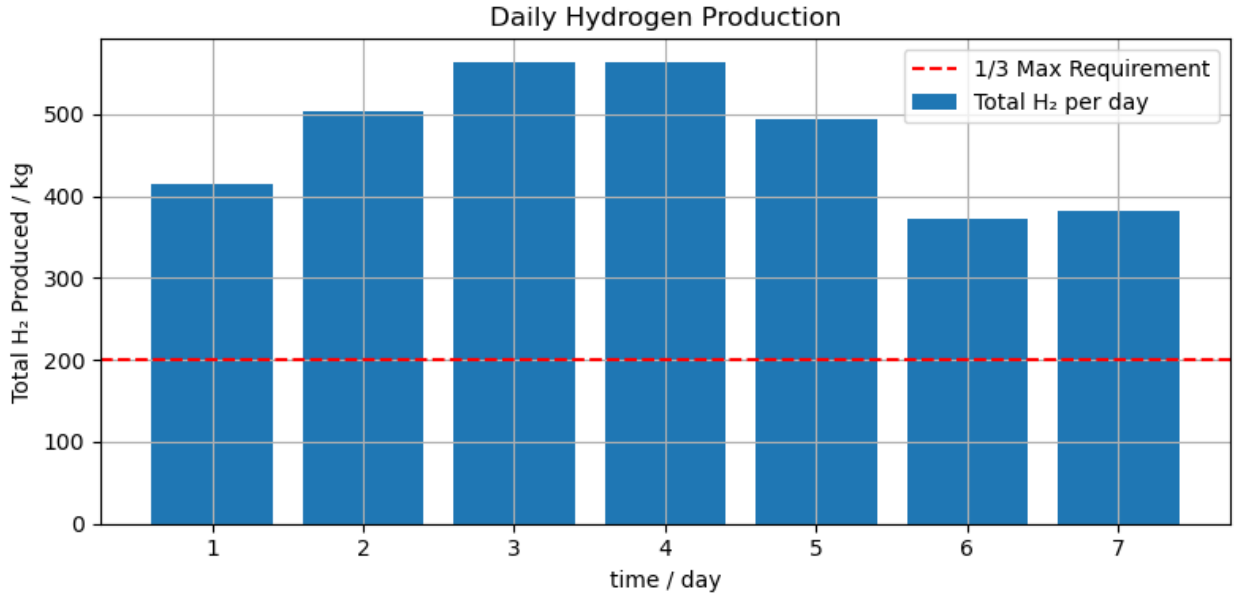

Figure A.22 - Daily hydrogen production for each simulation day and the respective production constraint in the expensive week obtained by CasADi for the PEM model in the grid price variation scenario

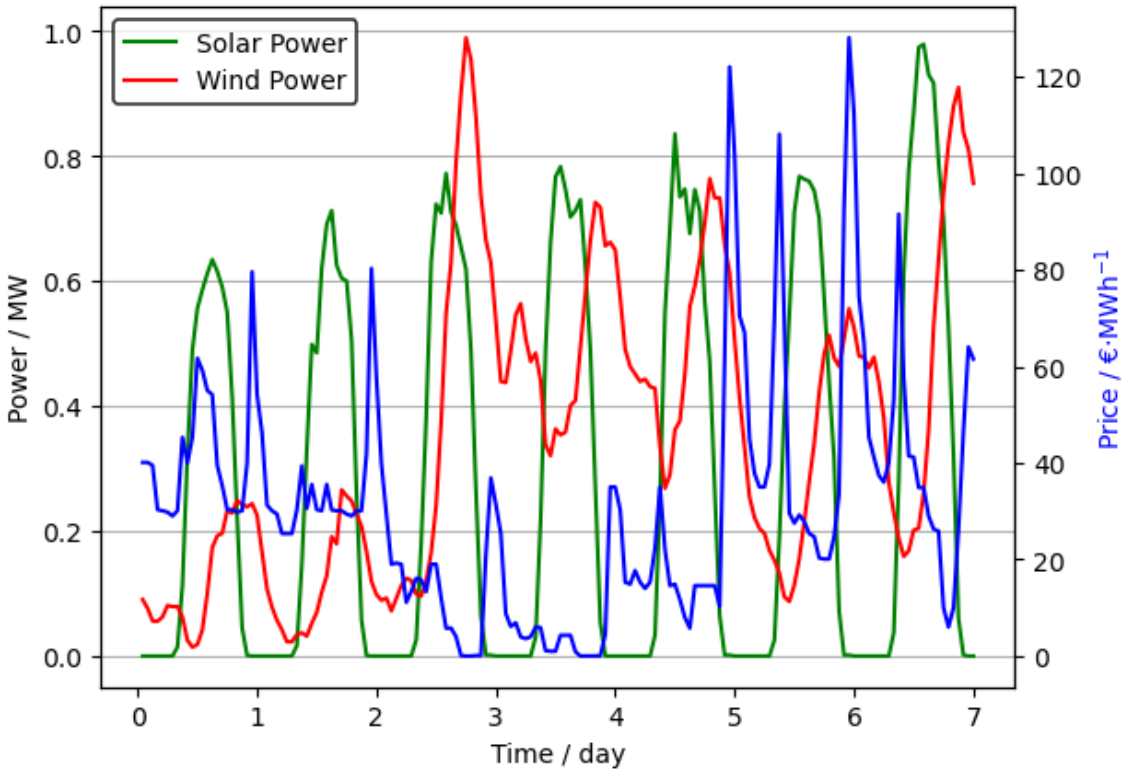

Figure A.23 - Renewable power and grid price histories in the expensive week obtained by CasADi for both models in the grid price variation scenario

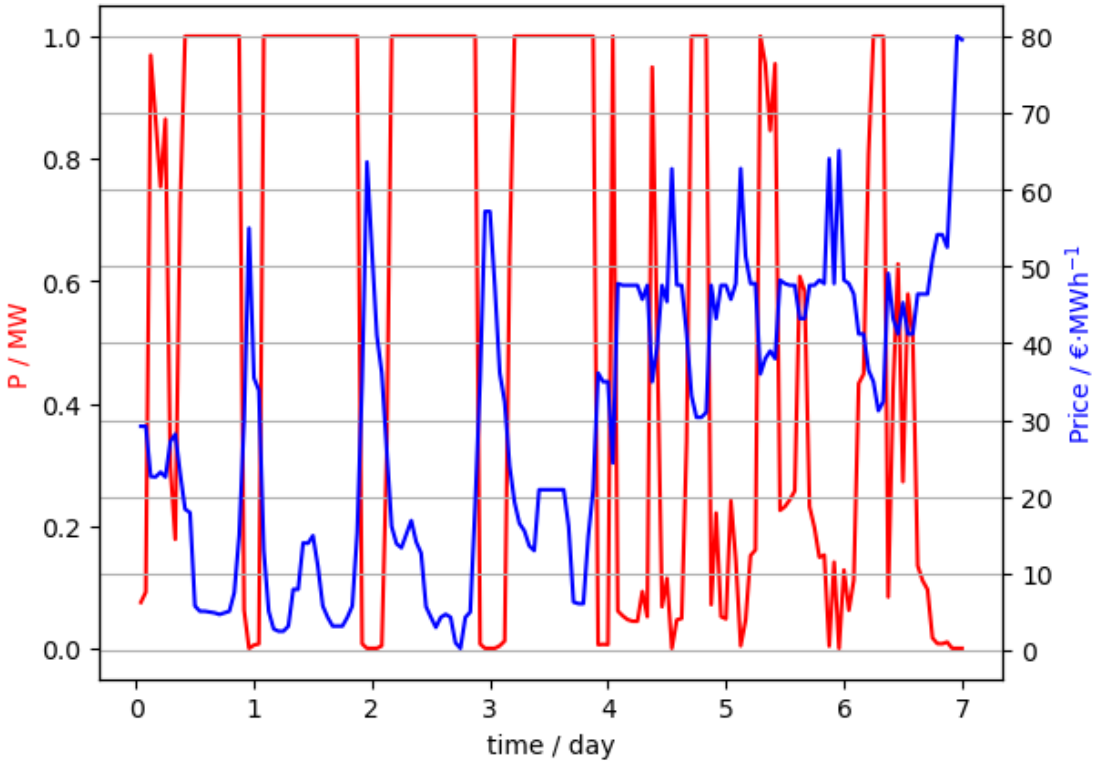

Figure A.24 - Electrolyzer power consumption and grid prices histories obtained by CasADi for the AWE model in the normal week with the hydrogen price reduction and grid price uncertainty

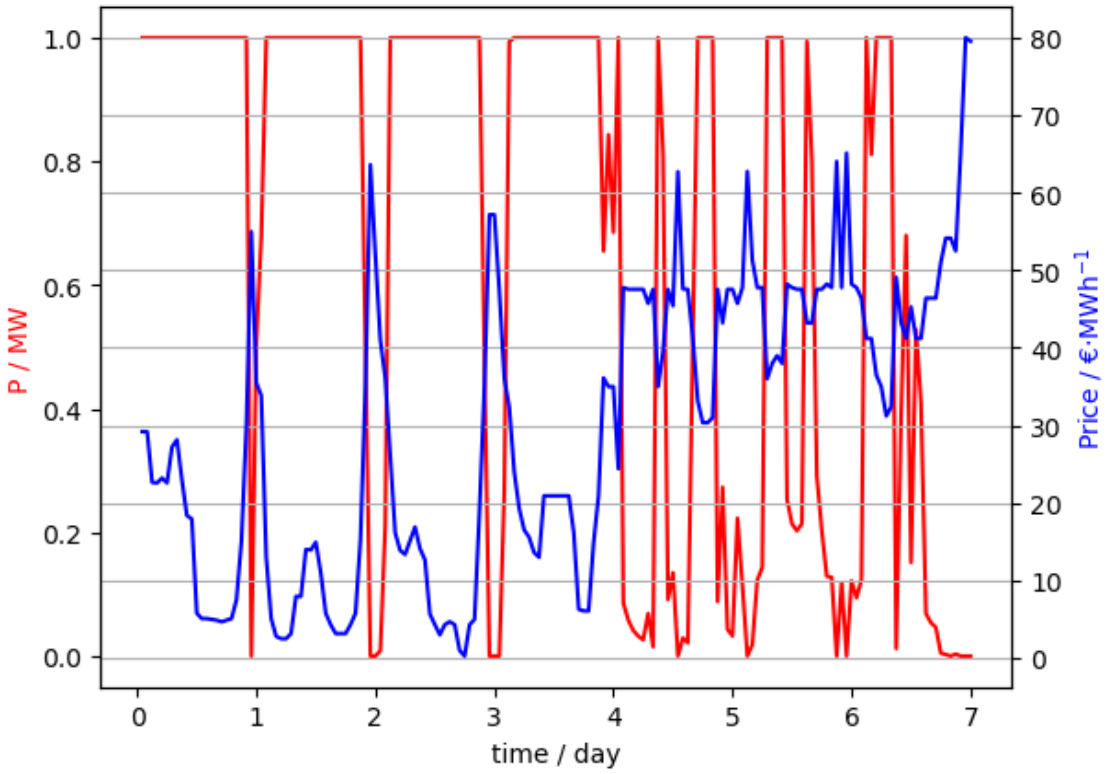

Figure A.25 - Electrolyzer power consumption and grid prices histories obtained by CasADi for the PEM model in the normal week with the hydrogen price reduction and grid price uncertainty